



Homocysteine impedes neurite outgrowth recovery after intracerebral haemorrhage by downregulating pCAMK2A

Guangyu Guo,¹ Jingfei Yang,¹ Wenliang Guo,¹ Hong Deng,¹ Haihan Yu,¹ Shuang Bai,¹ Gaigai Li,¹ Yingxin Tang,¹ Ping Zhang,¹ Yuming Xu ^{2,3}, Chao Pan,¹ Zhouping Tang ¹

To cite: Guo G, Yang J, Guo W, et al. Homocysteine impedes neurite outgrowth recovery after intracerebral haemorrhage by downregulating pCAMK2A. *Stroke & Vascular Neurology* 2023;8:e002165. doi:10.1136/svn-2022-002165

► Additional supplemental material is published online only. To view, please visit the journal online (<http://dx.doi.org/10.1136/svn-2022-002165>).

GG and JY are joint first authors.

Received 14 November 2022
Accepted 13 February 2023
Published Online First
28 February 2023



© Author(s) (or their employer(s)) 2023. Re-use permitted under CC BY-NC. No commercial re-use. See rights and permissions. Published by BMJ.

¹Department of Neurology, Tongji Hospital of Tongji Medical College of Huazhong University of Science and Technology, Wuhan, Hubei, China

²Department of Neurology, The First Affiliated Hospital of Zhengzhou University, Zhengzhou, Henan, China

³NHC Key Laboratory of Prevention and Treatment of Cerebrovascular Diseases, Zhengzhou, China

Correspondence to

Dr Zhouping Tang;
ddjtzp@163.com

Dr Chao Pan;
punctualpc@163.com

ABSTRACT

Hyperhomocysteinemia (HHcy) is independently associated with poorer long-term prognosis in patients with intracerebral haemorrhage (ICH); however, the effect and mechanisms of HHcy on ICH are still unclear. Here, we evaluated neurite outgrowth and neurological functional recovery using simulated models of ICH with HHcy in vitro and in vivo. We found that the neurite outgrowth velocity and motor functional recovery in the ICH plus HHcy group were significantly slower than that in the control group, indicating that homocysteine (Hcy) significantly impedes the neurite outgrowth recovery after ICH. Furthermore, phosphoproteomic data and signalome analysis of perihematomal brain tissues suggested that calmodulin-dependent protein kinases 2 (CAMK2A) kinase substrate pairs were significantly downregulated in ICH with HHcy compared with autologous blood injection only, both western blot and immunofluorescence staining confirmed this finding. Additionally, upregulation of pCAMK2A significantly increased neurite outgrowth recovery in ICH with HHcy. Collectively, we clarify the mechanism of HHcy-hindered neurite outgrowth recovery, and pCAMK2A may serve as a therapeutic strategy for promoting neurological recovery after ICH.

INTRODUCTION

Affecting 2 million people worldwide each year, intracerebral haemorrhage (ICH) is a serious type of stroke, and more than two-thirds of survivors cannot maintain their activities of daily living.^{1–3} There are many factors affecting the risk and prognosis of ICH, and high plasma homocysteine (Hcy) concentration, also known as hyperhomocysteinemia (HHcy), is a notable risk factor.⁴ According to a recent outpatients cohort of stroke, 35% of them had a high level of plasma Hcy, making it a high concern to this population.⁵ In addition, a clinical study showed that HHcy was independently associated with a poorer 3-month clinical outcome in patients with ICH.⁶

Molecular mechanisms that contribute to HHcy-induced disease involve reactive

WHAT IS ALREADY KNOWN ON THIS TOPIC

⇒ Hyperhomocysteinemia (HHcy) is the risk factor for intracerebral haemorrhage (ICH) and is associated with poor prognosis, but its underlying molecular mechanisms affecting neural repair after ICH are still poorly understood.

WHAT THIS STUDY ADDS

⇒ By morphological and behavioural tests, we suggest that Hcy impedes neurite outgrowth and neurological recovery after ICH. Then, our findings further indicate that Hcy significantly downregulates the phosphorylation level of calmodulin-dependent protein kinases 2 (CAMK2A) after ICH, which is associated with neurite outgrowth.

HOW THIS STUDY MIGHT AFFECT RESEARCH, PRACTICE OR POLICY

⇒ Our findings show that pCAMK2A may serve as a key target for promoting neurological recovery after ICH, indicating novel therapeutic strategies for improving the prognosis of ICH with HHcy in the future.

oxygen species and endothelial dysfunction.⁷ Endothelial dysfunction may contribute to the increased risk of ICH. However, for most patients with ICH with neurological function dysfunction accompanied by HHcy, whether Hcy directly interferes with neural repair after ICH is unclear. Several studies have revealed that Hcy can perturb phosphoprotein homeostasis,^{8–9} and phosphorylation has important implications on the function of neurite outgrowth.^{10–11} Therefore, we speculated that Hcy could impede neurite outgrowth and neurological recovery after ICH for patients with HHcy through a disturbance of switch-like kinase-phosphoprotein cascades. To test this hypothesis, we separately constructed ICH with HHcy models in vitro and in vivo. Morphological and behavioural characteristics were measured to evaluate neurite outgrowth recovery and neurological

function. To elucidate the mechanism of Hcy function on neurite outgrowth after ICH at a systemwide level, we used a global phosphoproteomic approach combined with proteomics. We explored the regulation of neurite outgrowth by kinase-substrate signalome and identified the core signalling pathway and target which may serve as a switch-like molecule for neurite outgrowth regulated by Hcy. Finally, we examined and validated its regulatory effect on neurite outgrowth recovery after ICH. Overall, we demonstrate that Hcy can inhibit neurite outgrowth after ICH and identify disturbances in the signalling network caused by Hcy. Importantly, these findings may indicate novel therapeutic strategies for improving the prognosis of ICH with HHcy.

MATERIALS AND METHODS

Animals

Male C57BL/6 mice (aged 5 weeks old, 14–16 g) were used in this study and were provided by the Animal Center of Tongji Hospital of Tongji Medical College of Huazhong University of Science and Technology (Wuhan, China). The mice were housed under a specific temperature-controlled environment with a 12-hour light/12-hour dark cycle. The mice were randomly divided into four groups: (1) Ctrl+vehicle group, (2) HHcy+vehicle group, (3) Ctrl+ICH group and (4) HHcy+ICH group, in which mice in the Ctrl groups were fed an ordinary diet, mice in the HHcy groups were fed with 1.7% high methionine feed for 6 weeks,¹² mice in the ICH groups were stereotactically injected with autologous blood and mice in the vehicle groups were given a sham ICH operation. A total of 220 mice were used for MOST (n: 10×4 = 40), neurobehavioral tests (n: 8×4 = 32), proteome and phosphoproteome (n: 3×3×4 = 36, three mice were mixed for each sample), western blot analysis (n: 8×4 = 32 on days 3, 8×4 = 32 on days 14), immunofluorescence staining (n: 6×4 = 24) and plasma Hcy concentration analysis (n: 6×4 = 24). The mice were allowed free access to food and water throughout the experimental period. Six mice died after stereotactic injection with autologous blood.

Plasma Hcy concentration

After the mice were fed 1.7% high methionine feed for 4 and 6 weeks, blood was collected from the inner canthus vein. The concentration of plasma Hcy was measured by the Department of Laboratory Medicine of Wuhan Tongji Hospital.

ICH models

ICH was induced by the stereotactic injection of autologous blood into the basal ganglia as previously described.^{13 14} Briefly, male C57BL/6 mice were anaesthetised with pentobarbital sodium and positioned in a stereotaxic frame in a prone position (RWD Life Science, China) and a burr hole was drilled into the skull. Then, 20 µL of autologous blood from the medial canthus vein without any anticoagulants was injected into the right basal ganglia (coordinates 0.5 mm anterior, 2.0 mm lateral

and 3.5 mm ventral to the bregma) at a rate of 1 µL/min by a microinfusion pump (RWD Life Science, China). After injection, the needle was left in position for an additional 10 min to prevent reflux and then withdrawn slowly at a rate of 1 mm/min. After suturing the wounds, all animals were monitored and provided with sufficient food and water. Only mice in which ICH was successful, excluding asymptomatic or dead mice, were included in this study. Using the same dosage as that applied to induce ICH, the mice subjected to the sham operation were only injected with phosphate buffered saline (PBS) into the basal ganglia.

Magnetic resonance imaging

MRI scans were performed to observe the formation and size of the haematoma on the first and third days after the establishment of ICH models. The mice were anaesthetised, fixed with special mouse coils and put into a 3.0 T magnetic resonance machine. The scanning sequence was as follows: coronal position, T2WI, TR 1800 ms, TE 90 ms, 1 mm-thick slice with 0.1 mm interslice gap.

Neurobehavioural tests

All neurobehavioral tests, including modified neurological severity scores (mNSS) and rotarod (Ugo Basile, Comerio, Italy) tests,¹⁵ were blindly administered by a laboratory technician on days 1, 3, 7, 14 and 21. Before inducing ICH, the mice were trained to rotate the rod for three cycles a day with an accelerating rotational speed from 4 rpm to 40 rpm within 5 min for 3 days before the surgical operation. On the third day of training, the average retention time on the rotarod was recorded to obtain baseline latency, and mice with poor motor function were excluded. The retention time of each mouse on the rotarod was tested six times at each time point after the operation, and the maximum value was recorded.

Western blot

Western blot was performed as described previously^{16–18} and the mouse brain tissues were separated from the perihematomal region (within 1 mm from the edge of the haematoma) for this analysis. Tissues were lysed and homogenised in RIPA lysis buffer supplemented with PMSF (Beyotime Biotechnology, China). The concentration of total protein in tissues was determined using a bicinchoninic acid (BCA) assay (Beyotime Biotechnology, China). The proteins were separated by 10% sodium dodecyl sulfate polyacrylamide gel electrophoresis (SDS-PAGE) and transferred onto nitrocellulose membranes. Then, the membranes were blocked in 5% skim milk for 1 hour at room temperature and incubated with the following primary antibodies overnight at 4°C: anti-MAP-2 (1:1000, Cell Signaling Technology, USA), anti-synaptophysin (1:5000, Proteintech, China), anti-CAMK2 (1:1000, Cell Signaling Technology, USA), anti-pCAMK2 (1:1000, Cell Signaling Technology, USA), anti-β-actin (1:1000, Cell Signaling Technology, USA), anti-α-tubulin (1:1000, Cell Signaling Technology, USA) and anti-BDNF

(1:1000, Abcam, UK), followed by incubation with anti-rabbit IgG (H+L) (DyLight 800 Conjugate; Cell Signaling Technology, USA) or anti-mouse IgG (H+L) (DyLight 800 Conjugate; Cell Signaling Technology, USA) secondary antibody for 1 hour at room temperature. The bands were visualised with an Odyssey Infrared Imaging System (LI-COR, Lincoln, NE, USA) and analysed with ImageJ (National Institutes of Health, Bethesda, Maryland).

Immunofluorescence staining

The surgical procedures were described previously.¹⁶ Mice were anaesthetised and transcardially perfused continuously with saline and 4% paraformaldehyde (PFA) solution. The brains were collected and postfixed for 24 hours in 4% PFA at 4°C and then dehydrated using 15% and 30% sucrose. Then, 30 µm slices of brain tissues were cut with a microtome (Leica CM1950, Germany). The cultured neurons were fixed with 4% PFA for 20 min and washed three times with PBS. The cells were incubated in 0.5% Triton X-100 for 30 min and blocked with 5% bovine serum albumin for 1 hour at room temperature. Then, cells were incubated overnight at 4°C with primary antibodies, including anti-MAP-2 (1:100, Cell Signaling Technology, USA), anti-pCAMK2 (Thr286) (1:100, Cell Signaling Technology, USA) and anti-βIII-tubulin (1:200, Cell Signaling Technology, USA), followed by secondary antibody incubation for 1 hour. Counterstaining was performed with 40,6-diamidino-2-phenylindole (DAPI; Beyotime, China). Cells were observed under an Olympus confocal laser scanning microscope (Olympus, Tokyo, Japan). Images were analysed with ImageJ software.

Golgi-Cox staining

Animals were anaesthetised and transcardially perfused with saline. Then, their whole brains were immediately removed on ice and placed in a brown glass bottle containing Golgi-Cox solution for fixation and impregnation. The Golgi-Cox solution contained 1% potassium dichromate, 1% mercuric chloride and 0.8% potassium chromate. The brains were stored at 4°C for 14 days, and the Golgi-Cox solution was replaced every 2 days. Afterward, the brains were immersed in a solution of 30% sucrose until they sank. The brains were then cut into 100 µm sections on a vibrating microtome (Leica CM1950, Germany), and the sections were attached to slides and dried. The sections were then dehydrated in 50%, 70%, 95% and 100% alcohol and immersed in CXA (chloroform/xylene/anhydrous ethanol) solution including chloroform, xylene and anhydrous ethanol at a volume ratio of 1:1:1. The sections were cover slipped and photographed by an automatic scanning microscope. The photos were processed using ImageJ software, and the density of dendrite spines was calculated and analysed.

Micro-optical sectioning tomography

Whole mouse brains were placed in a brown glass bottle with Golgi-Cox dye and stained for at least 2 months. Then, the brains were immersed in 1% lithium hydroxide for 24

hours, rinsed in distilled water for 24 hours, sequentially immersed in 50%, 70%, 85%, 95% and 100% alcohol, and 100% alcohol-acetone (1:1) for 2 hours and then transferred to a new brown jar (100% acetone) to dehydrate overnight. After dehydration, the brains were immersed in 50%, 75% and 100% Spurr resin for 8 hours and maintained in 100% Spurr resin for another 8 hours. After polymerisation, the brains were sectioned and imaged at a voxel size of $0.3 \times 0.3 \times 1 \mu\text{m}^3$ using the fast micro-optical sectioning tomography (fMOST) system¹⁹ to complete the brainwide data acquisition. Then, the fMOST images were obtained using the BioMapping3000/BioMapping5000 system (Oebio Biological, Wuhan, China). Image preprocessing was implemented using MATLAB and C++. For every brain, three $900 \times 900 \times 900 \mu\text{m}$ regions in the perihematomal tissue were reconstructed, and three neuronal cell bodies in each region were traced. Amira software (V.2020.1, FEI, Me'ignac Cedex, France) and Imaris software (V.9.7.2, Bitplane, Switzerland) were used to visualise the data and generate the figures and videos. The filament editor module of Amira was applied to the brainwide tracing of long-range axons in 3D by a combination of automated and manual approaches, and data blocks from the soma along the axons and dendrites were loaded into Amira. The initial and terminal points of fibres in the loaded blocks were assigned, and then Amira automatically calculated the path along which the fibre connected these two points.

Cell culture and treatment

We cultured primary cortical neurons as previously described.¹⁶ Briefly, cortical tissues were dissected from neonatal C57BL/6 mice and cut into pieces (1 mm^3), and then the cells were dissociated with 0.125% trypsin (Invitrogen, USA) for 15 min at 37°C. After centrifugation, the cells were resuspended in Dulbecco's modified Eagle medium/Ham's F12 (DMEM/F12; Gibco, USA) supplemented with 10% fetal bovine serum, 1% penicillin/streptomycin and 1% L-glutamine (all from Gibco, USA). Then, the suspension solution was seeded on 24-well and 96-well culture plates, which were coated with $100.0 \mu\text{g}/\text{mL}$ poly-L-lysine (Sigma-Aldrich, USA) and incubated at 37°C in a humidified atmosphere of 5% CO_2 . Later, the DMEM/F12 medium was replaced after 4 hours, and 50% of the medium was refreshed every 3 days with maintenance medium, which included neurobasal medium supplemented with 2% B27, 1% penicillin/streptomycin and 1% L-glutamine (all from Gibco, USA).

To simulate experimental ICH in vitro, we added different concentrations of hemin (Sigma-Aldrich, USA) to cells cultured in 96-well culture plates for 24 hours on day 10 of growth and quantified the cell viability by the Cell Counting Kit-8 (CCK-8) assay (Dojindo, Japan). Then, we selected the hemin concentration ($40 \mu\text{M}$) at which the cell viability was 50%. In addition, the cells were exposed to 0.25 mM or 0.5 mM Hcy (Sigma-Aldrich, USA) or the vehicle for 48 hours. The cells were grouped into the following categories: (a) normal control, (b) hemin

(40 μ M), (c) hemin (40 μ M) plus Hcy (0.25 mM) and (d) hemin (40 μ M) plus Hcy (0.5 mM).

Cell viability assay

The cell viability of cortical neurons was determined using a CCK-8 assay (Dojindo, Japan). To evaluate the ICH model in vitro, the cells were exposed to 0, 10, 20, 30, 40, 50, 60, 70 or 80 μ M hemin (Sigma-Aldrich, USA) in 96-well culture plates for 24 hours. Then, 10 μ L of CCK-8 solution was added to each well. After incubating for 4 hours at 37°C, the absorbance at 450 nm was measured following the manufacturer's instructions. In addition, the cells were exposed to 0, 0.25, 0.5, 0.75, 1, 1.25 or 1.5 mM Hcy (Sigma-Aldrich, USA) in 96-well culture plates for 48 hours and then quantified.

Transfection experiments

Lentivirus expressing an shRNA targeting pCAMK2A and lentivirus selectively expressing pCAMK2A and calmodulin-dependent protein kinases 2 (CAMK2A) were obtained from GeneChem (Shanghai, China), which were respectively added to cortical neurons to downregulate or upregulate pCAMK2A or CAMK2A. According to the manufacturer's instructions, cells were seeded in the maintenance medium for 24 hours and transfected with lentivirus and HitransG A solution that can promote lentivirus to transfect cells efficiently for 12 hours. As a negative control, the empty vector expressing GFP was used. Then, cells were exposed to hemin (Sigma-Aldrich, USA) for 24 hours at day 10 or Hcy (Sigma-Aldrich, USA) for 48 hours.

Proteome and phosphoproteome

Sample preparation

After being anaesthetised, the mice were transcardially perfused with PBS. For each proteome sample, perihematomal tissue from three mice was collected and mixed, and 40 mg tissue was homogenised using grinding beads (stainless steel, Shanghai Jingxin Industrial Development) on a tissue grinder instrument (Shanghai Jingxin Industrial Development). We used RIPA lysis buffer (50 mM Tris-HCl, pH 7.4, 150 mM NaCl, 0.25% deoxycholic acid, 1% NP-40, 1% SDS) with protease and a phosphatase inhibitor cocktail (Halt™, Thermo Scientific) for protein extraction. Then, 4 volumes of acetone were added to precipitate proteins for 2 hours at –80°C and the samples were centrifuged for 30 min at 14000g. The pellets were then washed two times with 80% acetone. The protein pellets were resuspended in 8 M urea, and a BCA assay was used to determine the protein concentration. Equal masses of protein for each sample were reduced and alkylated by dithiothreitol (final concentration of 10 mM) and iodoacetamide (final concentration of 50 mM) for 1 hour and 45 min, respectively. Then, trypsin (Mass Spectrometry Grade, Promega) was added to the samples at 1:50 (trypsin weight: protein weight) for protein digestion at 37°C overnight. The next day, trypsin was added at 1:100 (trypsin weight: protein weight) and for a 2 hours incubation at 37°C. The digestion was

terminated by adding 10% trifluoroacetic acid (TFA) to adjust the pH to 4. One hundred micrograms of peptides were desalted by an Oasis HLB solid phase extraction (SPE) column (30 μ M, Waters), and the remaining digest of approximately 4 mg of peptides was subsequently used for phosphopeptide enrichment.

Phosphopeptide enrichment

The SPE-Ti-IMAC microspheres were purchased from J&K Scientific, Ti(SO₄)₂ was purchased from Sinopharm Group, and 50 g Ti(SO₄)₂ and 1 g SPE-Ti-IMAC microspheres were used for the phosphopeptide enrichment of 12 samples. Ti⁴⁺ was immobilised in the microspheres by the previously reported method²⁰ to obtain the Ti⁴⁺-IMAC material. The material was packed into 1 mL SPE cartridges (30 μ M sieve plate) as a Ti⁴⁺-IMAC SPE column. The SPE procedure included four common steps: first, the SPE column was washed with 0.1% TFA for three volumes of solid phase, then, the digests were mixed with an equal volume of loading buffer (80% Acetonitrile (ACN)/6% TFA water solution) and loaded onto the column. We then used wash buffer 1 (50% ACN/6% TFA/200 mM NaCl) to remove the nonphosphopeptides on microspheres while wash buffer 2 (30% ACN/0.1% TFA) was used to remove the salt. After the final washing step, elution buffer (10% ammonium solution) was used to elute the phosphopeptides from the microspheres. The elution was evaporated to dryness. Before mass spectrometry (MS) analysis, 1% formic acid (FA) was used to redissolve it.

Liquid chromatography-MS analysis

Peptides of all the proteome samples were separated and analysed on an Easy-nLC 1200 UHPLC (Thermo Fischer Scientific) coupled with a Q Exactive HF-X mass spectrometer (Thermo Fischer Scientific). The trap column was 3 cm×150 μ m while the analytical column was 25 cm×150 μ m, and both were packed in-house with Repro Sil-Pur C18-AQ (1.9 μ m, Dr. Maisch GmbH). A Thermo stainless steel nanobore emitter was used.

The gradient mobile phase was generated by solvent A (0.1% FA) and solvent B (0.1% FA in 80% ACN) at 55°C and applied at a 600 nL/min flow rate for 120 min. The initial mobile phase contained 4% solvent B, and then the fraction of the B phase increased to 7% in 1 min. In the following 94 min, it increased to 25%; after another 16 min, it increased from 25% to 40% and then to 100% after an additional 5 min, where it remained for 4 min.

MS data acquisition was performed in positive ion and data-dependent acquisition modes. All full MS spectra were acquired in a scan range of 350–2000 m/z at a resolution of 60 k. Then, the 20 most intense multiple-charged ions (excluding eight and above) were selected for high energy collision dissociation (HCD) fragmentation and acquired at a resolution of 15 k. The normalised collision energy was 28.

MS data analysis

Raw data files generated from MS analysis were imported into Proteome Discovery software (V.2.4) for protein identification and label-free quantification. The reviewed fasta database of *Mus musculus* and the common contaminants database were downloaded from UniProt.org (July 2019). Most of the search parameters were set as default, except for the following: carbamidomethylation (+57.021 Da) of cysteine residues was set as a fixed modification; acetylation (+42.011 Da) of the protein N-terminal, oxidation (+15.995 Da) of methionine and phosphorylation (+79.966 Da) of serine, threonine and tyrosine were set as the dynamic modifications.

The mass tolerance for precursor ions was set to 10 ppm and for fragment ions to 0.6 Da. The number of maximum missed cleavage sites was set to 5. All searches were performed in Trypsin/P-specific digestion mode. The false discovery rate was strictly controlled to 0.01 at both the peptide and protein levels. Label-free quantification was used for comparisons between groups.

Data processing and downstream analysis

The protein and peptide (phosphorylation) quantification information was imported into R software (V.4.0.1) for downstream analysis. The *limma* package was used for differential expression analysis. The gene ontology (GO) analyses were performed using the R package *ClusterProfiler*. *Cytoscape* was used to perform *ClueGO*.²¹ To construct the signalome network, kinase–substrate relationship analyses were performed with the R package *PhosR*.

Statistical analysis

All the results are presented as the mean±SE of the mean (SEM) and were statistically analysed using GraphPad Prism V.8.0 (GraphPad Software, San Diego, California). Student's *t* tests (two-tailed) were used for the single comparisons, and one-way analysis of variances (ANOVAs) were used for the multiple comparisons of data with normal distribution (Shapiro-Wilk tests) and equal variance (*F* test). The data without normal distribution were analysed by Kruskal-Wallis tests for the multiple comparisons. The repeated-measures ANOVA was used to investigate differences in means across groups with repeated observations over time. When the ANOVA revealed significant differences, post hoc Bonferroni or Dunn's (following Kruskal-Wallis) tests were used to examine pairwise comparisons of means. *p*<0.05 was considered statistically significant.

RESULTS

Hcy inhibits neurite outgrowth after ICH

According to our study design (online supplemental figure S1), we first explored the effect of Hcy on primary cortical neurons treated with 40 µM hemin, which mimics the phenotype of ICH.²² The concentrations of hemin and Hcy were determined by CCK8 assay. Approximately 50% of cortical neurons treated with 40 µM hemin and 0.5 mM Hcy survived and the injured neurites gradually

recovered (online supplemental figure S2A-B, figure 1A). To assess the neurite outgrowth recovery, the total length, number and mean length of branches were measured. Compared with normal cortical neurons, neurite branches were significantly destroyed 2 days after hemin treated, the total length (187.98±2.94 µm vs 321.94±5.94 µm), the mean length (41.74±0.68 µm vs 54.02±1.16 µm) and the number (3.94±0.07 vs 6.86±0.17) of neurites were significantly decreased (figure 1B–D). In addition, the cortical neurons treated with 40 µM hemin and 0.5 mM Hcy had a worsen morphological indication compared with those treated with 40 µM hemin only at 2 days (total length, 102.92±2.80 µm vs 187.98±2.94 µm; mean length, 35.39±0.83 µm vs 41.74±0.68 µm; the number of branches, 2.80±0.06 vs 3.94±0.07). The neurite outgrowth recovered gradually with time, and the length, number and mean length of cortical neurons treated by hemin only at 4 days were significantly better than those treated by hemin plus Hcy (total length, 271.46±4.01 µm vs 146.46±3.17 µm; mean length, 49.53±0.93 µm vs 44.85±0.80 µm; number of branches, 5.79±0.13 vs 3.46±0.09), meanwhile they were also superior to cortical neurons treated with hemin only at 2 days (total length, 271.46±4.01 µm vs 187.98±2.94 µm; mean length, 49.53±0.93 µm vs 41.74±0.68 µm; number of branches, 5.79±0.13 vs 3.94±0.07). Even though there was an increasing trend of neurite outgrowth between cortical neurons treated with hemin plus Hcy at 4 days and 2 days, there was no significant difference, which means Hcy may impede neurite outgrowth recovery after the attack of ICH. Moreover, Sholl analysis showed that cortical neurons treated with hemin plus Hcy had fewer intersections between the neurites and Sholl circles compared with hemin treated only (figure 1E).

We further investigated the effect of Hcy on neurite outgrowth recovery using a mouse model of ICH with HHcy. The HHcy model was established by feeding mice with a high methionine diet containing 1.7%.²³ After 4 weeks of feeding, the Hcy level of mice fed with high-methionine diet increased fourfold compared with those in an ordinary diet (21.0±4.1 µM vs 5.1±1.1 µM). The ICH model was induced after 6 weeks of high-methionine diet, and the concentration of Hcy exceeded 70 µM (online supplemental figure S2C). We evaluated the volume of haematoma using T2-weighted imaging (online supplemental figure S2D), and there was no significant difference between ICH mice plus high-methionine diet (HHcy+ICH) and ICH mice plus ordinary diet (Ctrl+ICH). To evaluate the neurite outgrowth recovery at a global level, modified whole-brain Golgi staining and a micro-optical sectioning tomography (MOST) system were used to acquire the fine structure of neurons.²⁴ Neurons of the caudoputamen, hippocampal formation and basolateral amygdalar nucleus were reconstructed (figure 1F). We collected the neurite branch density in different brain regions, which was calculated by dividing the total length of neurites and the volume of different reconstructed regions (figure 1G–I). Still, the same trends persisted in animal models compared 14 days with 3 days, while the neurite branch density in HHcy+ICH was significantly less than

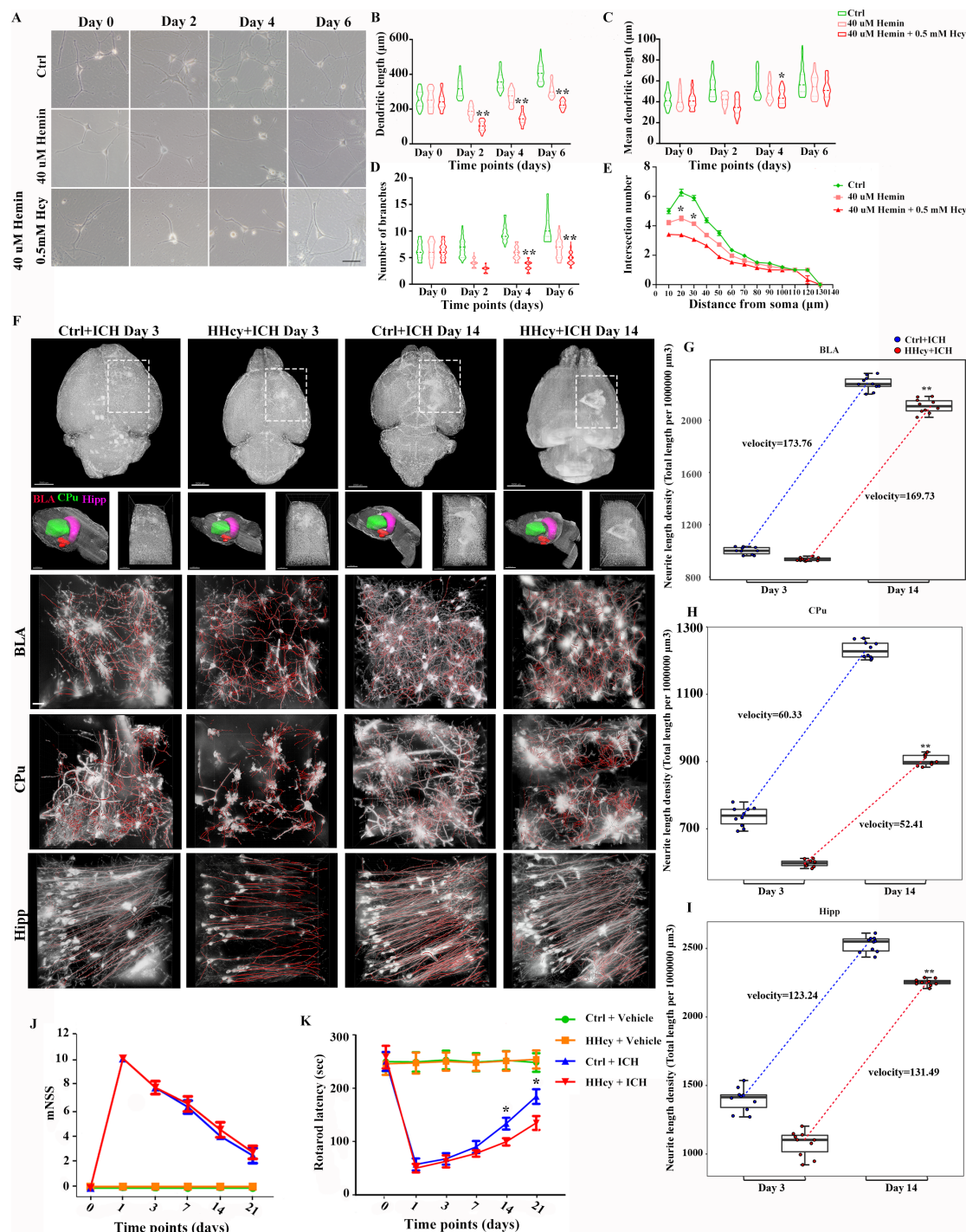


Figure 1 Hcy impedes neurite outgrowth after ICH in vitro and in vivo. (A) Primary cortical neurons were treated with hemin only or combined with Hcy. Cells were observed at different time points under a light microscope. The total length of neurites (B), the mean length of neurites (C) and the number of branches of neurites (D) were measured. $n=50\sim120/\text{group}$. (E) Sholl analysis for neurite complexity at day 6. $n=50\sim120/\text{group}$. $*p<0.05$, $**p<0.01$, 40 μM hemin versus 40 μM Hemin+0.5 mM Hcy treatment in (B) through (E). (F) Representative 3D reconstruction pictures of mouse brains by MOST in the HHcy+ICH and Ctrl+ICH groups on days 3 and 14, respectively. Row 3, 4 and 5: Detail 'blocks' in the Basolateral amygdalar nucleus (BLA), Caudoputamen (CPu) and Hippocampal formation (Hippo). Row 1: bar=2000 μm ; row 2: bar=1500 μm ; row 3–5: bar=40 μm . (G–I), Neurite branch length density: total length of neurite branches in the block/the volume of the block. $n=10/\text{group}$. $**p<0.01$, HHcy+ICH group vs Ctrl+ICH group. Neurological function was assessed using a modified Neurological Severity Score (J) or Rotarod test (K). $n=8/\text{group}$. $*p<0.05$, HHcy+ICH group versus Ctrl+ICH group. Statistical significance was calculated with the two-tailed unpaired Student's t tests in (B) through (E), one-way ANOVA/Tukey's tests or Kruskal-Wallis tests in (G) through (I) and Mann-Whitney U tests in (J) and (K). Data are presented as the mean \pm SEM. ANOVA, analysis of variance; Ctrl, control; Hcy, homocysteine; HHcy, hyperhomocysteinemia; ICH, intracerebral haemorrhage; MOST, micro-optical sectioning tomography.

Ctrl+ICH group at 3 days and 14 days after ICH. Additionally, the velocity of the neurites branches density increased was calculated by dividing the changes of neurite branch density between different times and time intervals, the HHcy+ICH group had a reduced velocity. Moreover, neurological functional outcomes at different time points were evaluated using the mNSS and rotarod test (figure 1J–K). An increase in mNSS and a decrease in rotarod latency occurred in the ICH model, and the neurological function after ICH gradually recovered with the progress of time, which was characterised by a reduction of the mNSS score and an increase in rotarod latency. Also, the defect of neurological function in HHcy+ICH was significantly more serious than Ctrl+ICH group at 14 days and 21 days after ICH. To verify the differences in neurite outgrowth recovery between HHcy+ICH and Ctrl+ICH group, the quantification of microtubule-associated protein-2 (MAP-2) and synaptophysin protein expression levels was detected by western blot (online supplemental figure S2E–G), which are the markers of neurites.^{25 26} The expression of MAP-2, a marker of neurons, was significantly reduced in HHcy+ICH mice 14 days after ICH compared with that of Ctrl+ICH mice. Meanwhile, the expression level of synaptophysin showed the same trend. Both cellular and animal models show that Hcy inhibits neurite outgrowth after ICH.

Hcy strongly alters the phosphorylation status of proteins associated with neurite outgrowth after ICH

To investigate the precise mechanisms of Hcy on neurite outgrowth, label-free proteome and IMAC-based phosphoproteome were acquired and analysed (figure 2A). We identified a total of 3348 proteins and 3188 phosphoproteins, meanwhile, overlapping data from phosphoproteome and proteome profiling revealed 1924 proteins (figure 2B). Figure 2C,D represented the protein and phosphoprotein levels across different groups. A total of 256 proteins and 69 phosphoproteins were found to be significantly altered in HHcy+ICH group compared with Ctrl+ICH group, while only seven proteins changed both their levels and phosphorylation levels (figure 2E, online supplemental table 1,2). GO enrichment analysis was carried out on upregulated and downregulated (phospho)proteins. The levels of proteins associated with actin filament organisation (GO:0007015), animal organ regeneration (GO:0031100) and positive regulation of response to wounding (GO:1903036) were downregulated significantly in HHcy+ICH group compared with Ctrl+ICH group, meanwhile, downregulated phosphoproteins by Hcy mainly were associated with regulation of actin filament depolymerisation (GO:0030834) and regulation of supramolecular fibre organisation (GO:1902903). The changes in actin filament are important to neurite outgrowth.²⁷ In contrast, there were no significantly enriched biological pathways for the upregulated proteins or phosphoproteins by Hcy after ICH.

Kinase substrate analysis reveals that CAMK2A plays an important role in Hcy-induced phosphorylation disturbance

Uncovering potential kinase-substrate pairs hidden in the phosphoproteome is important for interpreting the underlying biological significance of phosphoproteome data. Here, by using a multistep kinase-substrate scoring method reported by Yang *et al*,^{28 29} a signalome was constructed to identify discrete protein modules with similar kinase regulation and phosphorylation profiles. According to the signalome data (figure 3A–C), five distinct modules (1, 2, 3, 4 and 5) existed across four groups. Moreover, the signalome map highlighted that module 5 was entirely regulated by Ca^{2+} /CAMK2A and that the others were coregulated by several kinases. Most phosphosites of module 5 were downregulated in HHcy+ICH group (online supplemental figure S3), and gene set enrichment analysis (GSEA) revealed that module 5 was significantly associated with signalling for regulation of cell shape and neuron projection maintenance (figure 3D). These findings suggest that phosphorylation of CAMK2A may be a key molecular switch for neurite outgrowth, which was turned off by Hcy after ICH.

Hcy significantly downregulates the phosphorylation level of CAMK2A after ICH

The results of previous proteomics and phosphoproteomics studies revealed that Hcy might regulate the CAMK2A kinase-substrate group (figure 3, online supplemental figure S3). Thus, we examined the levels of CAMK2A and phospho-CAMK2A on the third-day post-ICH through the western blot (figure 4A–E). The western blot data showed that the level of pCAMK2A and pCAMK2B was increased in the Ctrl+ICH group compared with that in the Ctrl+vehicle group at 3 days and that the level decreased under HHcy treatment. However, no significant difference was found in the expression level of CAMK2A among HHcy+ICH group and Ctrl+Vehicle group (figure 4A–E). Additionally, after cortical neurons were treated with hemin for 24 hours and cultured with different concentrations of Hcy for 48 hours, decreased phosphorylation level of CAMK2A was observed through immunofluorescence staining (figure 4F–G).

Considering that brain-derived neurotrophic factor (BDNF) is a key downstream target of CAMK2 to promote neurite outgrowth,³⁰ we detected the expression level of BDNF by western blot (figure 4H–I). Results showed that Hcy significantly downregulated BDNF levels after ICH.

Upregulation of CAMK2A reverses the inhibition of neurite outgrowth after ICH by Hcy

To further explore the value of pCAMK2A as a potential therapeutic target for promoting neurite outgrowth after ICH with HHcy, lentivirus expressing a shRNA targeting pCAMK2A and lentivirus selectively expressing pCAMK2A and CAMK2A were obtained, which were used to downregulate or upregulate pCAMK2A or CAMK2A. According to immunofluorescence staining data (figure 5A–D), the length and number of neurite branches were significantly

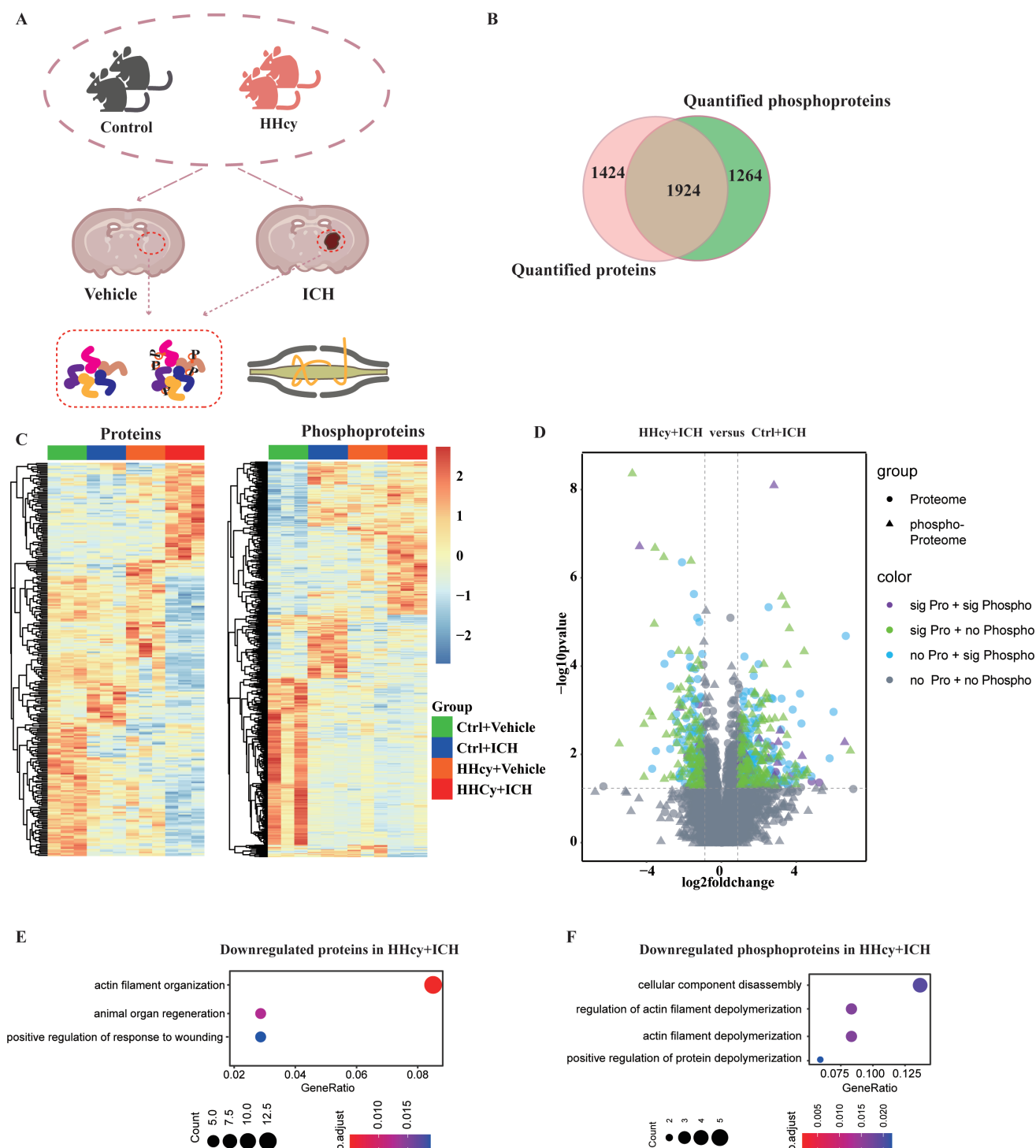


Figure 2 Hcy downregulates proteins and phosphoproteins associated with neurite outgrowth. (A) Flowchart of the experimental design to collect proteome and phosphoproteome. (B) The overlap relationships between proteins and phosphoproteins detected by LC-MS/MS. (C) Heatmaps reveal differently expressed proteins and phosphoproteins analysis among groups. The colour bar represents the expression levels. (D) Volcano plot of proteome and phosphoproteome data. Data are represented as log (2) fold change for the HHcy+ICH group compared with that of the Ctrl+ICH group. The origins represent levels of proteins from the proteome, and small triangles represent the phosphoprotein levels. The colour of the dots represents the significance levels of proteins and phosphoproteins. Purple dots, sig Pro+sig Phospho, the proteins are both significantly changed in the proteome and phosphoproteome; green dots, no Pro+sig Phospho, the proteins are significantly changed in phosphorylation levels, but there were no significant changes in protein levels; sky blue dots, the proteins are significantly changed in protein levels, but there were no significant changes in phosphoprotein levels; grey dots, there were no significant changes in the proteome and phosphoproteome. GO enrichments for proteins (E) and phosphoproteins (F) downregulated in HHcy+ICH versus Ctrl+ICH groups. Ctrl, control; GO, gene ontology; Hcy, homocysteine; HHcy, hyperhomocysteinemia; ICH, intracerebral haemorrhage; LC-MS/MS, liquid chromatograph mass spectrometer.

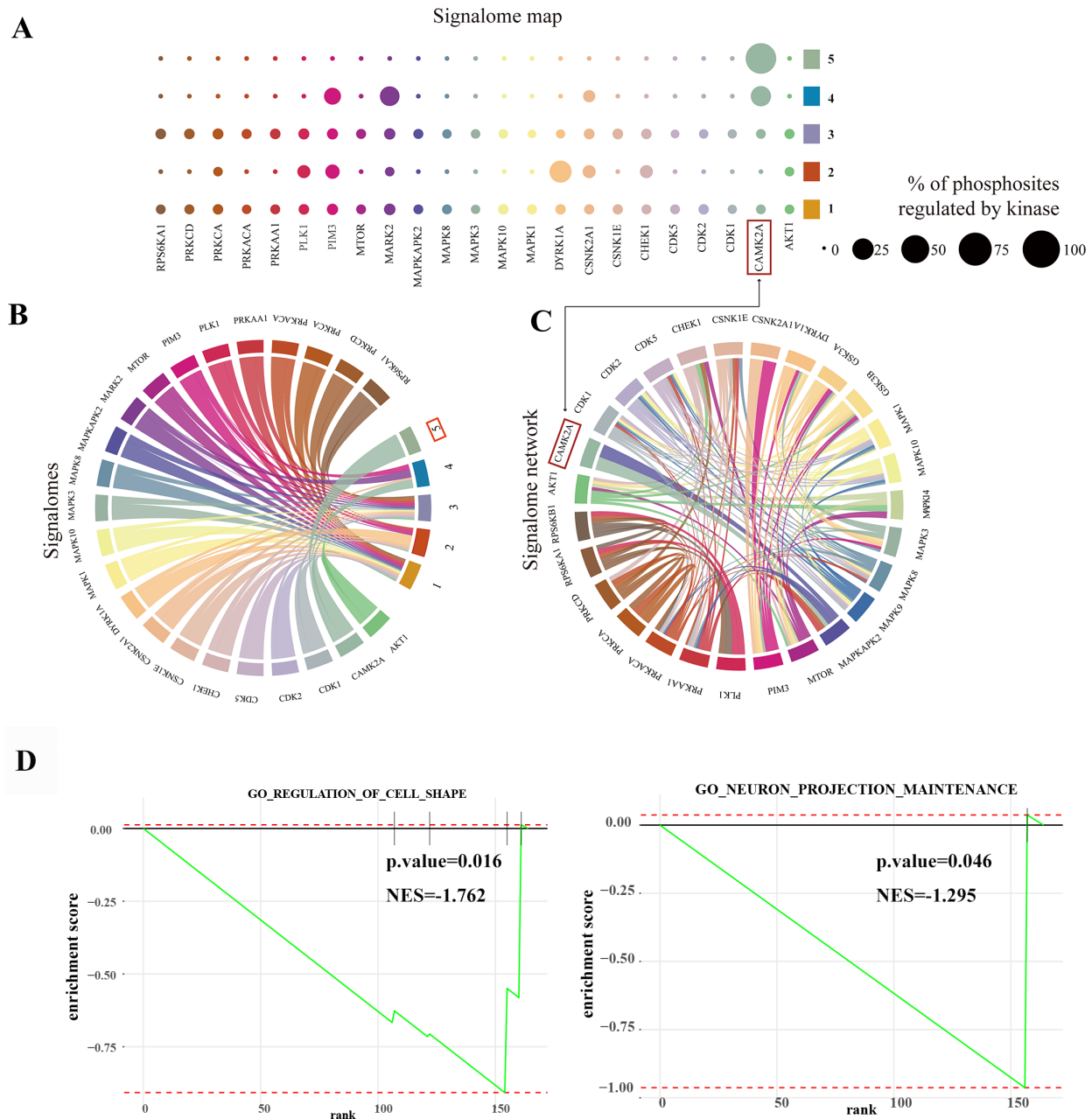


Figure 3 Construction of the signalome across different groups using the phosphoproteome. (A,B) The signalome map identified 23 kinases that make up the branches, and five phosphosite modules consisted of the stem nodes with a distinct regulatory profile. The bubble chart displays the proportion of phosphosite modules regulated by different kinases. Module 5 was fully regulated by CAMK2A. (C) A network of interactions among kinases. (D) The changes between HHcy+ICH and Ctrl+ICH were enriched by gene sets enrichment analysis. Ctrl, control; HHcy, hyperhomocysteinemia; ICH, intracerebral haemorrhage; NES, normalised enrichment score.

reduced when exposed to hemin and Hcy compared with those of hemin treatment alone. Interestingly, the elevated protein or phosphorylation levels of CAMK2A increased the length and number of neurite branches. This finding suggests that CAMK2A plays an important role in neurite outgrowth after ICH. Meanwhile, on reducing the level of phosphorylated CAMK2A, the complexity of neurites was comparable to that of the cotreatment group with hemin and Hcy. These results suggest that pCAMK2A may be a potential target to promote neurite outgrowth in convalescent patients with ICH with HHcy.

DISCUSSION

In the present study, we found that Hcy could impede neurite outgrowth and neurological function recovery after ICH. Using the quantitative phosphoproteome together with a global proteome analysis, we revealed for the first time that Hcy affected the protein phosphorylation alterations associated with neurite outgrowth. Through in vitro and in vivo experiments, we confirmed that Hcy significantly inhibited neurite outgrowth after ICH through decreasing phosphorylation of CAMK2A. This is the first study to report the inhibitory effect of

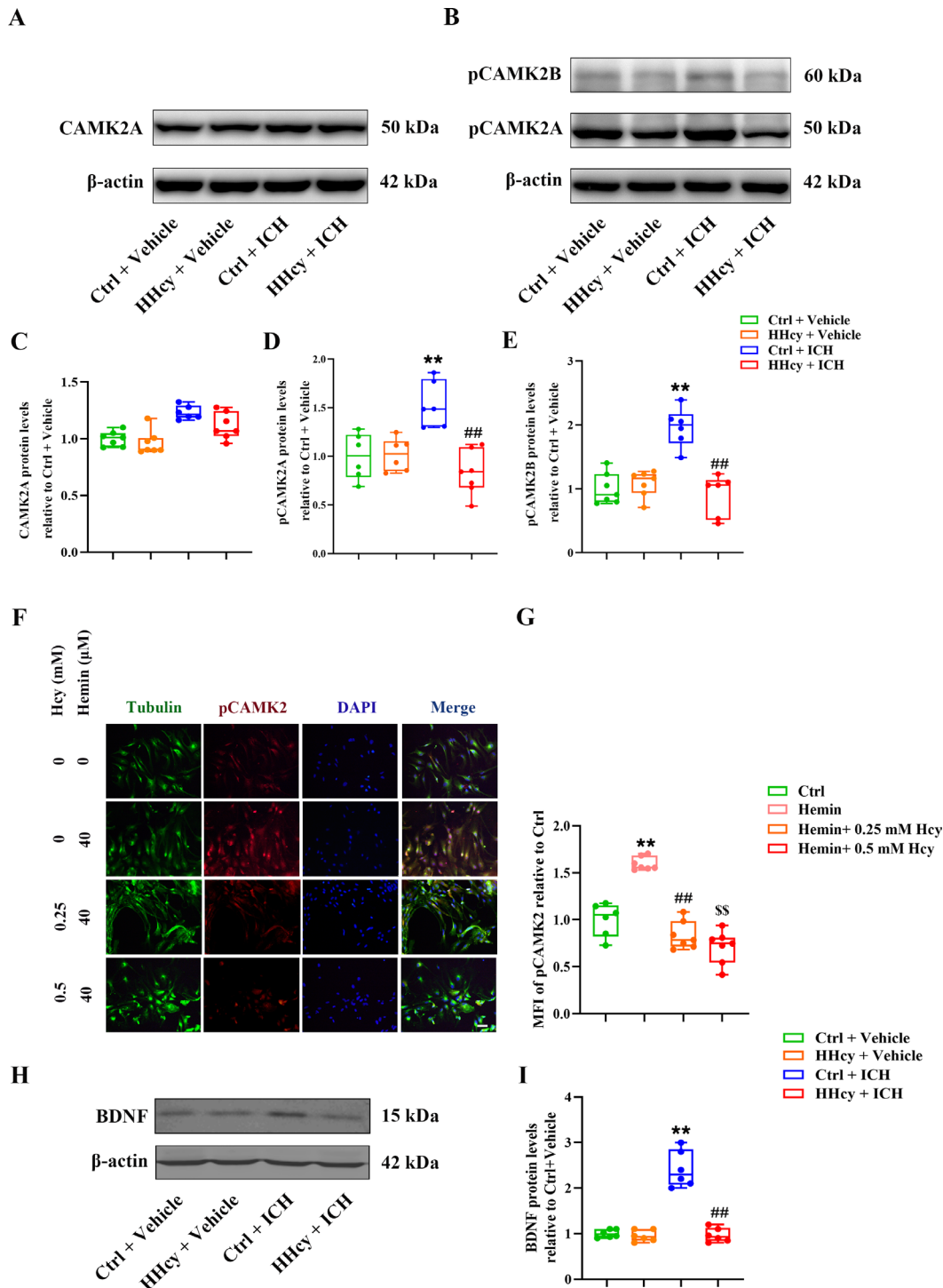


Figure 4 Hcy significantly downregulates the phosphorylation level of CAMK2A after ICH. (A,B) Total CAMK2, phosphorylated (p) CAMK2A and pCAMK2B were detected by Western blot in the Ctrl+Vehicle, HHcy+Vehicle, Ctrl+ICH and HHcy+ICH groups on day 3. (C) through (E) Quantification of CAMKII, p-CAMK2A and p-CAMK2B protein expression levels relative to the Ctrl+Vehicle group by Western blot. $n=6\sim7/\text{group}$. (F) After exposure to hemin for 24 hours and two concentrations of Hcy for 48 hours, cortical neurons were assessed by immunofluorescence with pCAMK2 (red), β -tubulin III (green), and DAPI (blue) staining. Scale bar=50 μm . (G) Quantification of the MFI of pCAMK2 from (F). $n=6\sim7/\text{group}$. (H) BDNF was detected by Western blot in the Ctrl+Vehicle, HHcy+Vehicle, Ctrl+ICH and HHcy+ICH groups on day 3. (I) Quantification of BDNF protein expression levels relative to the Ctrl+Vehicle group from (H) is shown. $n=6/\text{group}$. Statistical significance was calculated with one-way ANOVA/Tukey's tests or Kruskal-Wallis tests in (C) through (E), (G) and (I). Data are presented as the mean \pm SEM. ** $p<0.01$, Ctrl+ICH group versus Ctrl+Vehicle group; ## $p<0.01$, HHcy+ICH group versus Ctrl+ICH group in (C) through (E) and (I). ** $p<0.01$, 40 μM Hemin group versus Ctrl group; ##, \$\$\$ $p<0.01$, 40 μM Hemin+0.25 mM or 0.5 mM Hcy group versus 40 μM Hemin group in (G). ANOVA, analysis of variance; Ctrl, control; Hcy, homocysteine; HHcy, hyperhomocysteinemia; ICH, intracerebral haemorrhage; MFI, mean fluorescence intensity.

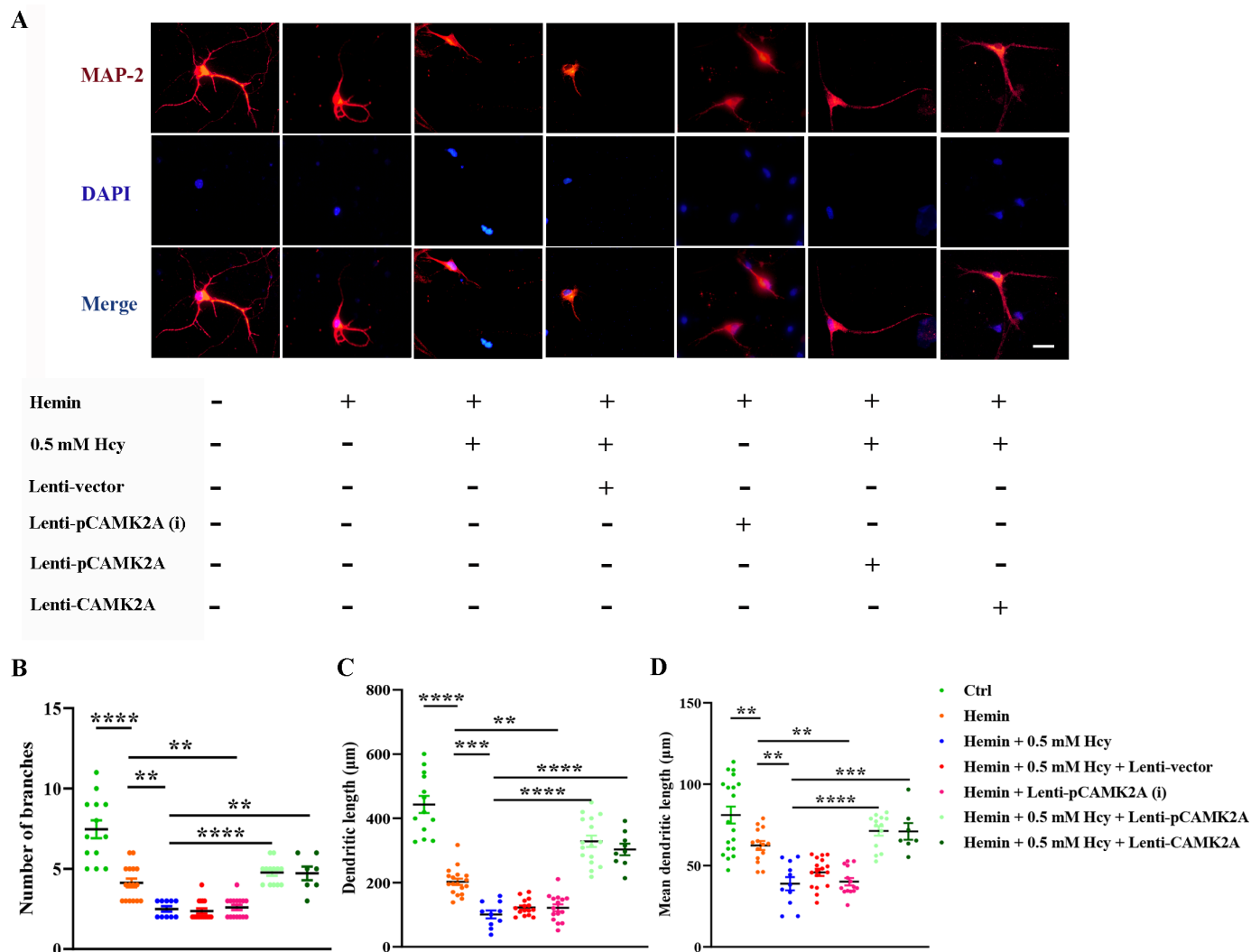


Figure 5 Upregulation of pCAMK2A reverses the inhibition of neurite outgrowth after ICH by Hcy. (A) After exposure to hemin for 24 hours and Hcy (0.5 mM) for 48 hours, cortical neurons treated with Lenti-pCAMK2A(i), Lenti-pCAMK2A and Lenti-CAMK2A for 12 hours were assessed by immunofluorescence with MAP2 (red) and DAPI (blue) staining. Lenti-pCAMK2A(i) treatment downregulated the level of pCAMK2A by mutating protein phosphorylation site (S286) to positively charged alanine, Lenti-pCAMK2A treatment upregulated the level of pCAMK2A by mutating protein phosphorylation site (S286) to negatively charged aspartic acid. Scale bar=50 μ m. The number of branches of neurites (B), the total length of neurites (C) and the mean length of neurites (D) were measured. $n=7\sim 19$ /group. Statistical significance was calculated with the one-way ANOVA/Tukey's tests or Kruskal-Wallis tests in (B) through (D). Data are presented as the mean \pm SEM ** $p<0.01$, *** $p<0.001$, **** $p<0.0001$. ANOVA, analysis of variance; Ctrl, control; Hcy, homocysteine; ICH, intracerebral haemorrhage.

Hcy on neurite outgrowth recovery after ICH and the underlying mechanisms of this process. Accordingly, by promoting neurite outgrowth, pCAMK2A is a potential therapeutic target for patients with ICH with HHcy.

Elevated plasma concentration of Hcy, a sulfur-containing amino acid, has been shown in observational (cohort and case-control) studies and systematic reviews to be a potential risk factor for vascular diseases and stroke in particular. Reduction in Hcy levels is significantly associated with a reduced risk of first stroke,³¹ and high Hcy levels can predict higher recurrence and mortality in ischaemic stroke, especially in patients with the large-vessel atherosclerosis subtype.^{32,33} Experimental studies have also confirmed that HHcy has an impact on cerebral vascular biology, and its molecular mechanisms

include oxidative stress, proinflammatory pathways and endothelial dysfunction.³⁴ Additionally, Wang *et al* found that Hcy enhanced neural stem cell autophagy in in vivo and in vitro models of ischaemic stroke, which may be one of the molecular mechanisms of Hcy neurotoxicity.³⁵ In addition, elevated plasma Hcy concentration is associated not only with ischaemic stroke but also with haemorrhagic stroke. Several studies have shown that HHcy is independently associated with a higher risk of ICH, a larger haematoma volume, a poorer prognosis and a lower survival rate in patients with ICH.^{4,6,36-38} Neuroinflammation and the increased activity of the matrix metalloproteinase 2 (MMP2) and MMP9 systems induced by HHcy may underlie the pathogenesis of ICH.³⁹ Moreover, in our study, by using morphological and behavioural

experiments, we found more serious neurological deficits and decreased neurites branches density in ICH mice treated with HHcy (figure 1). Therefore, Hcy can inhibit neurite outgrowth recovery in ICH models, which may be one of the reasons for poor prognosis.

There is growing evidence that the protein phosphorylation induced by protein kinases is one of the primary mechanisms involved in the regulation of signal transduction pathways that control neurite outgrowth in the mammalian brain and, thus, affects motor control, sensory processing and synaptogenesis.^{40–42} Protein tyrosine kinases and many common serine/threonine kinases, such as cyclic adenosine monophosphate (cAMP)-dependent protein kinase, CAMK2 and Ca^{2+} /phospholipid-dependent protein kinase, are highly expressed in the central nervous system.^{40–42} Protein kinases can influence dendritic growth to form synaptic contacts and regulate neurite plasticity through the phosphorylation of specific substrates, and, thus, the dysregulation of kinases may perturb dendritic growth and synaptic function and lead to disease states.⁴³ Therefore, it is necessary to use the quantitative phosphoproteome together with a global proteome analysis to further explore the mechanism by which HHcy impedes neurite outgrowth recovery during ICH. We showed that several kinase families, such as CAMKs and mitogen-activated protein kinases, drive the changes in phosphosites caused by HHcy during ICH (figures 2 and 3). Moreover, among the related kinase families, we found that CAMK2A activity may be largely responsible for the inhibition of neurite outgrowth recovery mediated by Hcy (figures 4 and 5).

CAMK2, a Ser/Thr protein kinase, is critical in Ca^{2+} signal transduction and is highly enriched at the synapses in the brain tissue.⁴⁴ There are four isoforms of CAMK2 (α , β , γ and δ) encoded by four distinct but highly related genes (CAMK2A, CAMK2B, CAMK2G and CAMK2D).⁴⁵ Among them, the α and β isoforms of CAMK2 are the most abundant isoforms expressed in neurons⁴⁶ and CAMK2A has been identified as a central regulator of neuronal plasticity.⁴⁵ After Ca^{2+} enters the cell through N-methyl-D-aspartate receptors and binds to calmodulin (CaM), Ca^{2+} alters its conformation, and Ca^{2+} /CaM binds to CAMK2 to activate it by autonomous phosphorylation at T286 (on CAMK2B) or Thr287 (on CAMK2B), and this process contributes to many neuronal regulatory pathways.^{46–47} The substrates phosphorylated by CAMK2 include proteins that modulate presynaptic transmission as well as essential plasticity-regulating receptors and signalling molecules in the postsynaptic cells.⁴⁴ CAMK2 regulates presynaptic plasticity by limiting synaptic vesicle release.⁴⁶ One study reported that peripheral axon injury increased the phosphorylation level of CAMK2 and that activation of CAMK2-promoted neuronal axon growth in vitro, which demonstrates that CAMK2 is a critical modulator of mammalian axon regeneration.⁴⁸ In addition, CAMK2 is important for dendrite development and dendritic spine formation.⁴³ We showed that the levels of

most phosphorylation sites of the CAMK2A substrate in ICH mice treated with HHcy were significantly lower than those of the control group, indicating that Hcy might regulate the CAMK2A kinase-substrate group and inhibit neurite outgrowth recovery. Furthermore, we found that pCAMK2A levels were upregulated in ICH mice and in vitro with hemin treatment. Through an experiment utilising primary neurons treated with hemin, Hcy and lentiviruses, we showed that the upregulation of CAMK2A and pCAMK2A expression reduced the inhibitory effect of Hcy on neurite outgrowth recovery and that the downregulation of pCAMK2A levels suppressed neurite outgrowth recovery in vitro with hemin treatment. Thus, based on our results, it is possible that the expression of pCAMK2A is upregulated in ICH but reduced by Hcy, and this may be the mechanism by which Hcy inhibits neurite outgrowth recovery and neurological recovery. Additionally, the nerve growth factor and neurotrophic drugs can stimulate nerve regrowth,⁴⁹ and BDNF signalling via its transmembrane receptor tropomyosin-related kinase B is essential for neuronal survival, differentiation and axonal growth.^{50–51} Studies have shown that CAMK2 can induce phosphorylation of cAMP response element-binding protein (CREB), which binds to a cAMP response element within genes and alters the expression of key proteins involved in neurite outgrowth, such as BDNF.^{52–54} Consistently, our results indicated that Hcy could inhibit the expression of BDNF in the perihematomal region after ICH (figure 4H,I). Therefore, we speculate that Hcy may inhibit neurite outgrowth through the CAMK2/BDNF pathway, which will be further explored in our subsequent study. However, our study had the limitation that in vivo experiments were not conducted to verify the effects of upregulation or downregulation of CAMK2A and pCAMK2A expression on neurite outgrowth recovery and neurological function in ICH mice. In addition, given the importance of elevated neurogenesis in the subventricular zone (SVZ) after stroke for neurological recovery,⁵⁵ we examined whether Hcy affects neurogenesis in the SVZ after ICH. We used immunofluorescence to assess the expression level of doublecortin (DCX) in the SVZ after ICH, which is normally expressed on NPCs and is considered a marker of neurogenesis in adulthood.⁵⁶ We found that the percentage of DCX+cells in the SVZ after ICH was significantly lower in the Hcy+ICH group than in the Ctrl+ICH group, indicating that Hcy might inhibit neural rehabilitation by suppressing neurogenesis after ICH, which needs further in-depth study (online supplemental figure S4).

In conclusion, our results demonstrate that Hcy can downregulate the levels of pCAMK2A and CAMK2 kinase-substrate group during ICH, which explains why Hcy inhibits neurite outgrowth in vivo and in vitro. This study may provide direct evidence for the potential of novel therapeutic targets to manage the neurotoxic effect of Hcy in patients with ICH with high Hcy levels.

Contributors GG and JY performed the experiments, analysed data and drafted the manuscript. WG and HD bred the mice and established the animal models. HY, SB and GL conducted some of the cell culture experiments. YT, PZ and YX participated in editing the manuscript. CP and ZT designed, supervised the study and guided the editing of manuscripts. And ZT is responsible for the overall content as the guarantor.

Competing interests None declared.

Patient consent for publication Not applicable.

Ethics approval All the experiments were approved by the Experimental Animal Ethics Committee of Huazhong University of Science and Technology, and the number of the ethical approval document is TJ-A20160805.

Provenance and peer review Not commissioned; externally peer reviewed.

Data availability statement Data are available in a public, open access repository. The proteomic data can be accessed from iProX database (<https://www.iprox.cn>) under accession number IPX0004967000. The datasets generated during this study will be available from the corresponding authors upon reasonable request.

Supplemental material This content has been supplied by the author(s). It has not been vetted by BMJ Publishing Group Limited (BMJ) and may not have been peer-reviewed. Any opinions or recommendations discussed are solely those of the author(s) and are not endorsed by BMJ. BMJ disclaims all liability and responsibility arising from any reliance placed on the content. Where the content includes any translated material, BMJ does not warrant the accuracy and reliability of the translations (including but not limited to local regulations, clinical guidelines, terminology, drug names and drug dosages), and is not responsible for any error and/or omissions arising from translation and adaptation or otherwise.

Open access This is an open access article distributed in accordance with the Creative Commons Attribution Non Commercial (CC BY-NC 4.0) license, which permits others to distribute, remix, adapt, build upon this work non-commercially, and license their derivative works on different terms, provided the original work is properly cited, appropriate credit is given, any changes made indicated, and the use is non-commercial. See: <http://creativecommons.org/licenses/by-nc/4.0/>.

ORCID iDs

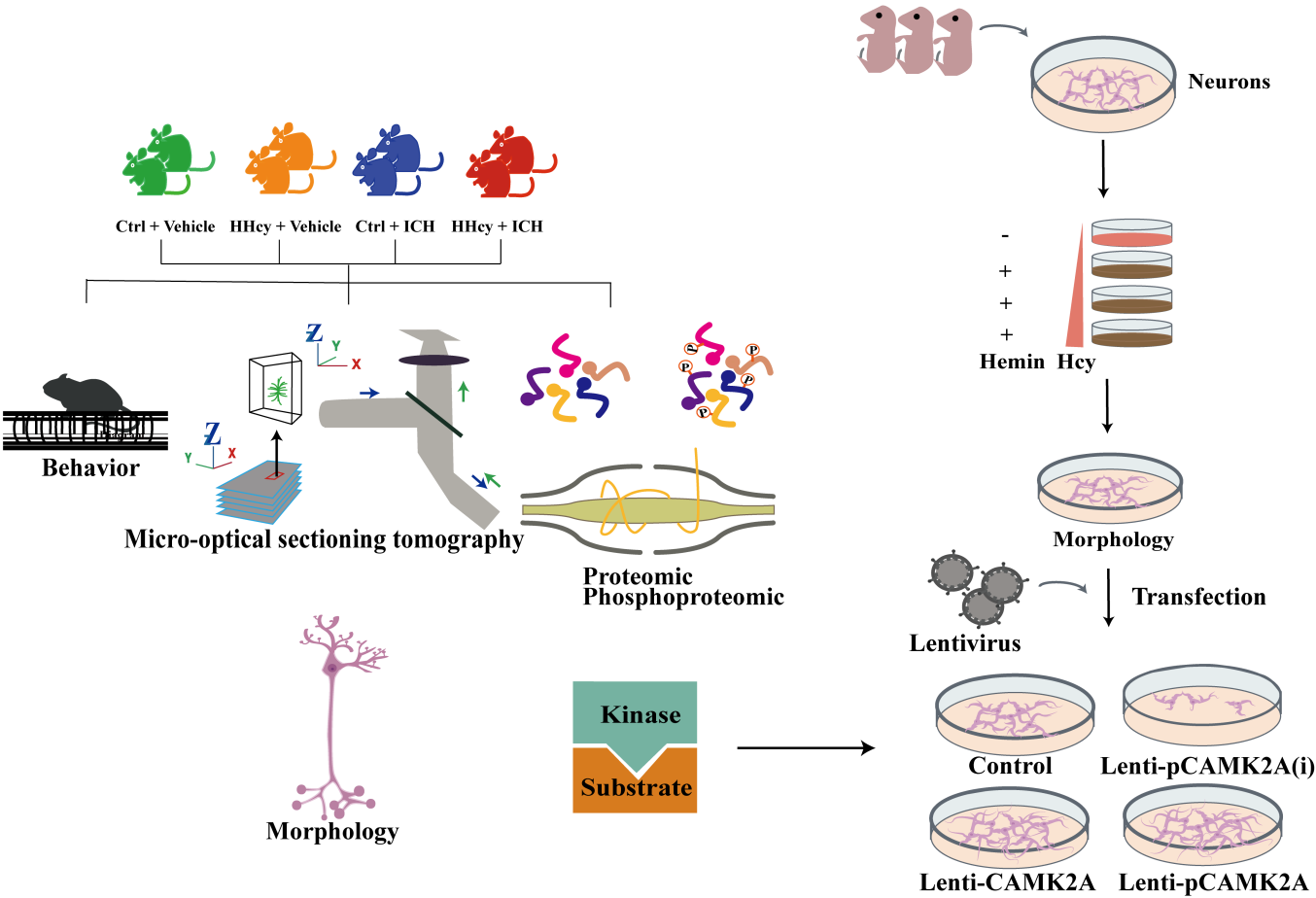
Yuming Xu <http://orcid.org/0000-0003-2689-9897>

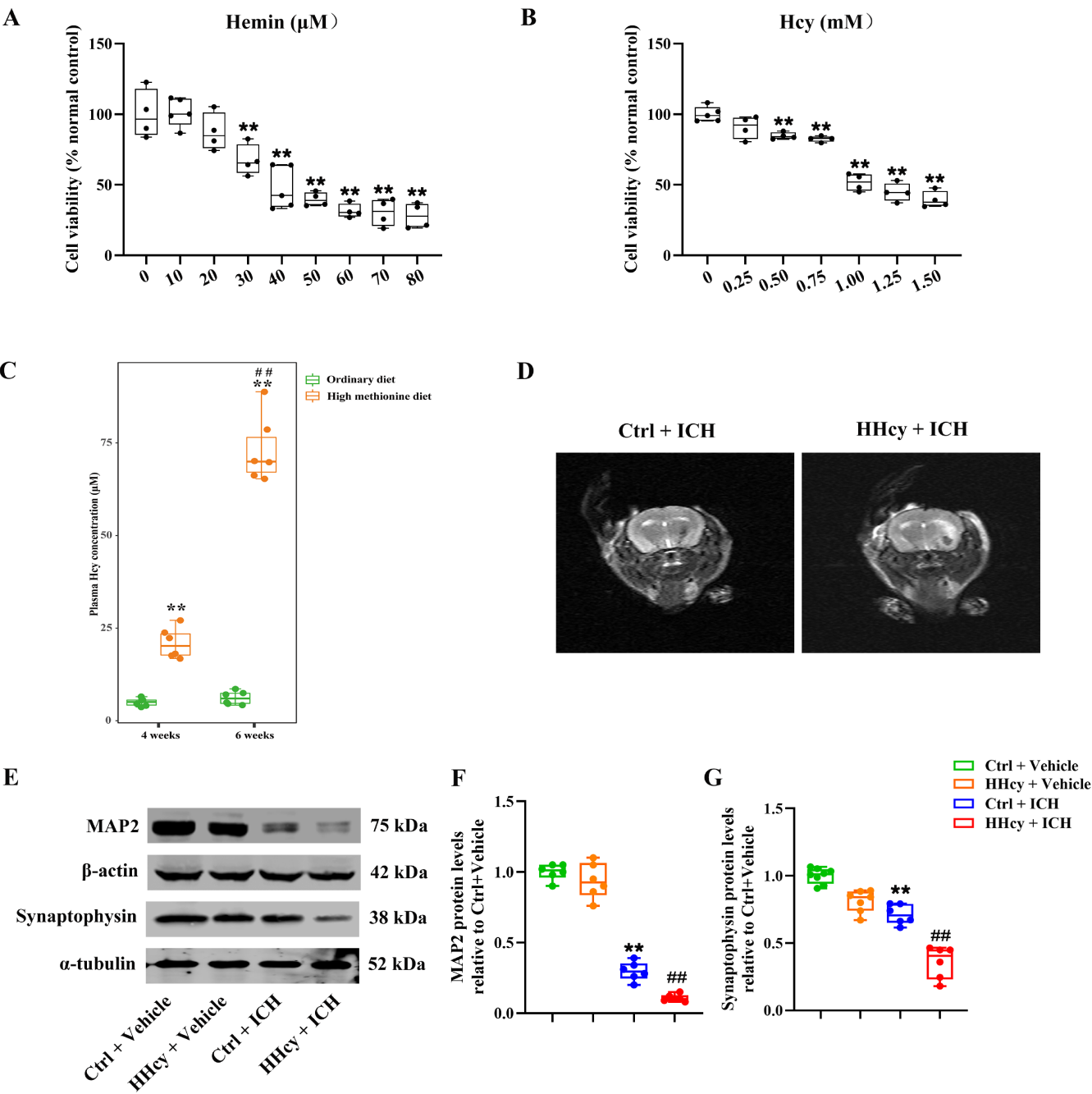
Zhouping Tang <http://orcid.org/0000-0002-4153-8590>

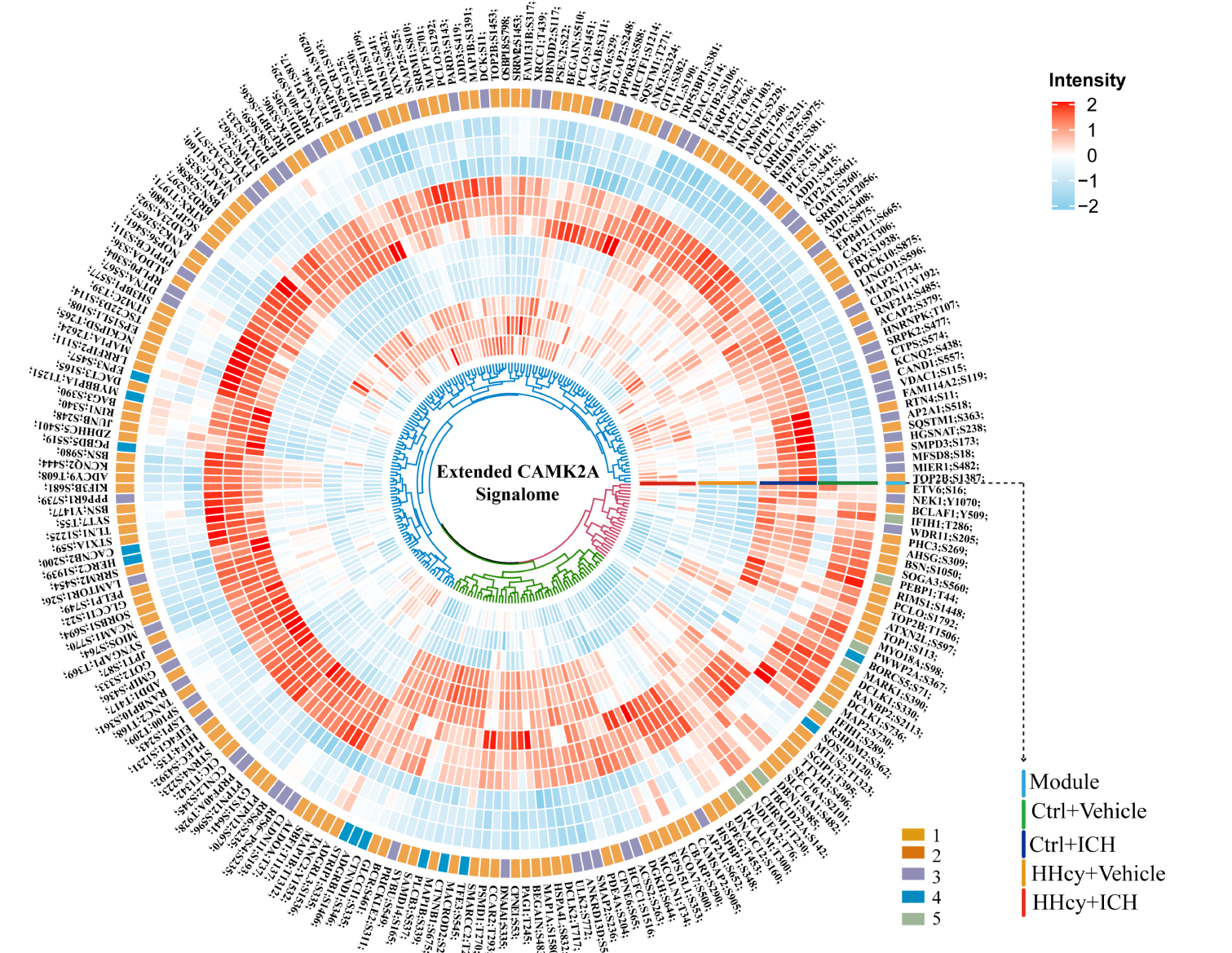
REFERENCES

- Krishnamurthi RV, Feigin VL, Forouzanfar MH, *et al.* Global and regional burden of first-ever ischaemic and haemorrhagic stroke during 1990-2010: findings from the global burden of disease study 2010. *Lancet Glob Health* 2013;1:e259-81.
- Cordonnier C, Demchuk A, Ziai W, *et al.* Intracerebral haemorrhage: current approaches to acute management. *Lancet* 2018;392:1257-68.
- Xi G, Keep RF, Hoff JT. Mechanisms of brain injury after intracerebral haemorrhage. *Lancet Neurol* 2006;5:53-63.
- Li Z, Sun L, Zhang H, *et al.* Elevated plasma homocysteine was associated with hemorrhagic and ischemic stroke, but methylenetetrahydrofolate reductase gene C677T polymorphism was a risk factor for thrombotic stroke: a multicenter case-control study in China. *Stroke* 2003;34:2085-90.
- Ahmed S, Bogiatzi C, Hackam DG, *et al.* Vitamin B 12 deficiency and hyperhomocysteinemia in outpatients with stroke or transient ischaemic attack: a cohort study at an academic medical centre. *BMJ Open* 2019;9:e026564.
- Wang D, Wang W, Wang A, *et al.* Association of severity and prognosis with elevated homocysteine levels in patients with intracerebral hemorrhage. *Front Neurol* 2020;11:571585.
- Weiss N, Heydrick S, Zhang Y-Y, *et al.* Cellular redox state and endothelial dysfunction in mildly hyperhomocysteinemic cystathionine beta-synthase-deficient mice. *Arterioscler Thromb Vasc Biol* 2002;22:34-41.
- Signorello MG, Segantin A, Passalacqua M, *et al.* Homocysteine decreases platelet no level via protein kinase C activation. *Nitric Oxide* 2009;20:104-13.
- Shirafuji N, Hamano T, Yen S-H, *et al.* Homocysteine increases tau phosphorylation, truncation and oligomerization. *Int J Mol Sci* 2018;19:891.
- Haberberger RV, Barry C, Matusica D. Immortalized dorsal root ganglion neuron cell lines. *Front Cell Neurosci* 2020;14:184:184..
- Park SY, An JM, Seo JT, *et al.* Y-27632 induces neurite outgrowth by activating the nox1-mediated Akt and PAK1 phosphorylation cascades in PC12 cells. *Int J Mol Sci* 2020;21:7679.
- Shah DI, Singh M. Possible role of Akt to improve vascular endothelial dysfunction in diabetic and hyperhomocysteinemic rats. *Mol Cell Biochem* 2007;295:65-74.
- Bao W-D, Zhou X-T, Zhou L-T, *et al.* Targeting mir-124/ferroportin signaling ameliorated neuronal cell death through inhibiting apoptosis and ferroptosis in aged intracerebral hemorrhage murine model. *Aging Cell* 2020;19:e13235.
- Xiong X-Y, Liu L, Wang F-X, *et al.* Toll-Like receptor 4/myd88-mediated signaling of hepcidin expression causing brain iron accumulation, oxidative injury, and cognitive impairment after intracerebral hemorrhage. *Circulation* 2016;134:1025-38.
- Chen J, Li Y, Wang L, *et al.* Therapeutic benefit of intravenous administration of bone marrow stromal cells after cerebral ischemia in rats. *Stroke* 2001;32:1005-11.
- Pan C, Liu N, Zhang P, *et al.* Egb761 ameliorates neuronal apoptosis and promotes angiogenesis in experimental intracerebral hemorrhage via rsk1/gsk3 β pathway. *Mol Neurobiol* 2018;55:1556-67.
- Wang X, Liu D, Huang H-Z, *et al.* A novel microRNA-124/ptn1 signal pathway mediates synaptic and memory deficits in alzheimer's disease. *Biol Psychiatry* 2018;83:395-405.
- Li G, Yu H, Liu N, *et al.* Overexpression of CX3CR1 in adipose-derived stem cells promotes cell migration and functional recovery after experimental intracerebral hemorrhage. *Front Neurosci* 2019;13:462.
- Li A, Gong H, Zhang B, *et al.* Micro-optical sectioning tomography to obtain a high-resolution atlas of the mouse brain. *Science* 2010;330:1404-8.
- Yao Y, Dong J, Dong M, *et al.* An immobilized titanium (IV) ion affinity chromatography adsorbent for solid phase extraction of phosphopeptides for phosphoproteome analysis. *J Chromatogr A* 2017;1498:22-8.
- Shannon P, Markiel A, Ozier O, *et al.* Cytoscape: a software environment for integrated models of biomolecular interaction networks. *Genome Res* 2003;13:2498-504.
- Cheng J, Tang J-C, Pan M-X, *et al.* L-lysine confers neuroprotection by suppressing inflammatory response via microRNA-575/ptn signaling after mouse intracerebral hemorrhage injury. *Exp Neurol* 2020;327:113214.
- Suszyńska-Zajczyk J, Luczak M, Marczak L, *et al.* Hyperhomocysteinemia and bleomycin hydrolase modulate the expression of mouse brain proteins involved in neurodegeneration. *J Alzheimers Dis* 2014;40:713-26.
- Guo C, Long B, Hu Y, *et al.* Early-stage reduction of the dendritic complexity in basolateral amygdala of a transgenic mouse model of alzheimer's disease. *Biochem Biophys Res Commun* 2017;486:679-85.
- Bodakuntla S, Jijumon AS, Villablanca C, *et al.* Microtubule-associated proteins: structuring the cytoskeleton. *Trends Cell Biol* 2019;29:804-19.
- Veschani N, Yang J-L, Ngampramuan S, *et al.* Melatonin reverts methamphetamine-induced learning and memory impairments and hippocampal alterations in mice. *Life Sci* 2021;265:118844.
- Ciaffardini F, Nicolai S, Caputo M, *et al.* The Cockayne syndrome B protein is essential for neuronal differentiation and neuritogenesis. *Cell Death Dis* 2014;5:e1268.
- Yang P, Humphrey SJ, Cinghu S, *et al.* Multi-omic profiling reveals dynamics of the phased progression of pluripotency. *Cell Syst* 2019;8:427-45.
- Kim HJ, Kim T, Hoffman NJ, *et al.* PhosR enables processing and functional analysis of phosphoproteomic data. *Cell Rep* 2021;34:108771.
- Yan X, Liu J, Ye Z, *et al.* Camkii-Mediated CREB phosphorylation is involved in Ca²⁺-induced BDNF mRNA transcription and neurite outgrowth promoted by electrical stimulation. *PLoS One* 2016;11:e0162784.
- Huang X, Li Y, Li P, *et al.* Association between percent decline in serum total homocysteine and risk of first stroke. *Neurology* 2017;89:2101-7.
- Shi Z, Liu S, Guan Y, *et al.* Changes in total homocysteine levels after acute stroke and recurrence of stroke. *Sci Rep* 2018;8:6993.
- Shi Z, Guan Y, Huo YR, *et al.* Elevated total homocysteine levels in acute ischemic stroke are associated with long-term mortality. *Stroke* 2015;46:2419-25.
- Faraci FM, Lentz SR. Hyperhomocysteinemia, oxidative stress, and cerebral vascular dysfunction. *Stroke* 2004;35:345-7.
- Wang M, Liang X, Cheng M, *et al.* Homocysteine enhances neural stem cell autophagy in vivo and in vitro model of ischemic stroke. *Cell Death Dis* 2019;10:561.
- Zhou Z, Liang Y, Qu H, *et al.* Plasma homocysteine concentrations and risk of intracerebral hemorrhage: a systematic review and meta-analysis. *Sci Rep* 2018;8:2568.

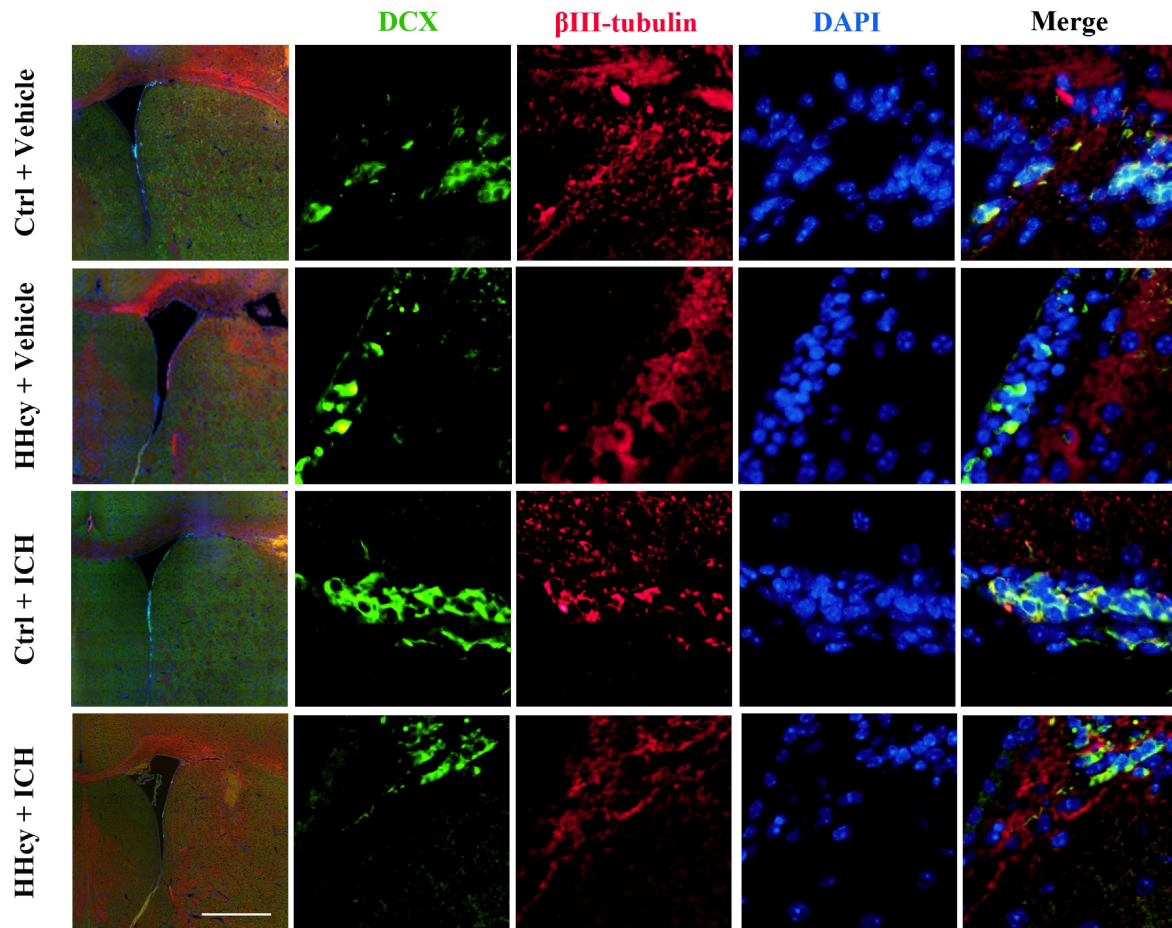
- 37 Zhou F, Chen B, Chen C, *et al.* Elevated homocysteine levels contribute to larger hematoma volume in patients with intracerebral hemorrhage. *J Stroke Cerebrovasc Dis* 2015;24:784–8.
- 38 Li Q, Zhao Z, Si K, *et al.* Correlation between the levels of NLRP3, hcy, IL-1 β , IL-18 and the prognosis in patients with hemorrhagic stroke. *Am J Transl Res* 2021;13:2883–90.
- 39 Sudduth TL, Powell DK, Smith CD, *et al.* Induction of hyperhomocysteinemia models vascular dementia by induction of cerebral microhemorrhages and neuroinflammation. *J Cereb Blood Flow Metab* 2013;33:708–15.
- 40 Raymond LA, Blackstone CD, Huganir RL. Phosphorylation of amino acid neurotransmitter receptors in synaptic plasticity. *Trends Neurosci* 1993;16:147–53.
- 41 Hawasli AH, Bibb JA. Alternative roles for Cdk5 in learning and synaptic plasticity. *Biotechnol J* 2007;2:941–8.
- 42 Huganir RL, Greengard P. Regulation of neurotransmitter receptor desensitization by protein phosphorylation. *Neuron* 1990;5:555–67.
- 43 Nourbakhsh K, Yadav S. Kinase signaling in dendritic development and disease. *Front Cell Neurosci* 2021;15:624648.
- 44 Hudmon A, Schulman H. Neuronal Ca²⁺/calmodulin-dependent protein kinase II: the role of structure and autoregulation in cellular function. *Annu Rev Biochem* 2002;71:473–510.
- 45 Nicole O, Pacary E. Camkii β in neuronal development and plasticity: an emerging candidate in brain diseases. *Int J Mol Sci* 2020;21:7272.
- 46 Moro A, van Woerden GM, Toonen RF, *et al.* Camkii controls neuromodulation via neuropeptide gene expression and axonal targeting of neuropeptide vesicles. *PLoS Biol* 2020;18:e3000826.
- 47 Sałaciak K, Koszałka A, Żmudzka E, *et al.* The calcium/calmodulin-dependent kinases II and IV as therapeutic targets in neurodegenerative and neuropsychiatric disorders. *Int J Mol Sci* 2021;22:4307.
- 48 Xi F, Xu R-J, Xu J-H, *et al.* Calcium/Calmodulin-Dependent protein kinase II regulates mammalian axon growth by affecting F-actin length in growth cone. *J Cell Physiol* 2019;234:23053–65.
- 49 Chen L, Chen T, Mao G, *et al.* Clinical neurorestorative therapeutic guideline for brainstem hemorrhage (2020 china version). *Journal of Neurorestoration* 2020;8:232–40.
- 50 Esvald E-E, Tuvikene J, Sirp A, *et al.* Creb family transcription factors are major mediators of BDNF transcriptional autoregulation in cortical neurons. *J Neurosci* 2020;40:1405–26.
- 51 Harward SC, Hedrick NG, Hall CE, *et al.* Autocrine BDNF-TrkB signalling within a single dendritic spine. *Nature* 2016;538:99–103.
- 52 Sheng M, Thompson MA, Greenberg ME. CREB: A ca(2+)-regulated transcription factor phosphorylated by calmodulin-dependent kinases. *Science* 1991;252:1427–30.
- 53 Tao X, Finkbeiner S, Arnold DB, *et al.* Ca²⁺ influx regulates BDNF transcription by a CREB family transcription factor-dependent mechanism. *Neuron* 1998;20:709–26.
- 54 Shieh PB, Hu SC, Bobb K, *et al.* Identification of a signaling pathway involved in calcium regulation of BDNF expression. *Neuron* 1998;20:727–40.
- 55 Zhao Y, Guan Y-F, Zhou X-M, *et al.* Regenerative neurogenesis after ischemic stroke promoted by nicotinamide phosphoribosyltransferase-nicotinamide adenine dinucleotide cascade. *Stroke* 2015;46:1966–74.
- 56 Couillard-Despres S, Winner B, Schaubeck S, *et al.* Doublecortin expression levels in adult brain reflect neurogenesis. *Eur J Neurosci* 2005;21:1–14.



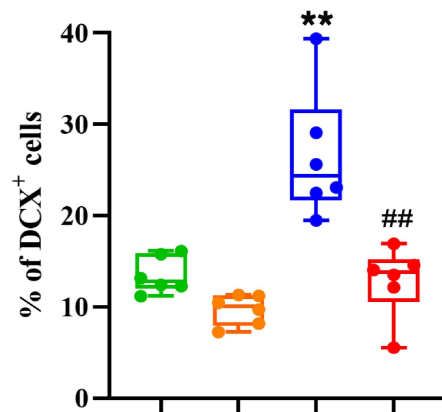




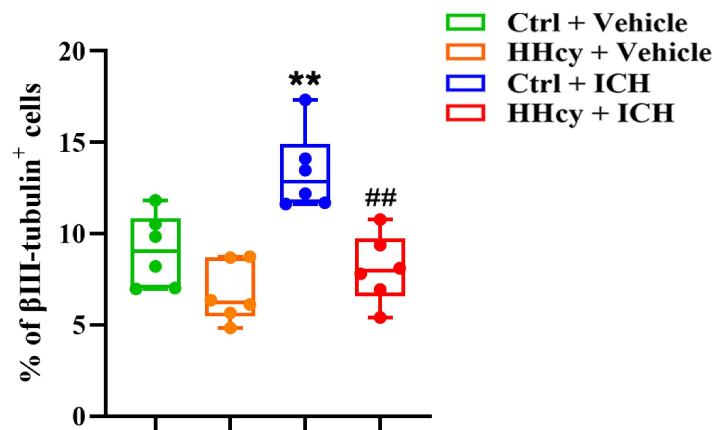
A



B



C



Accession	Entrez	Gene	Ensembl	Gene	Symbols	log2FC	p. value	p. adjust.	direction
Q921I1	22041	ENSMUSG00C	Trf			-2.680639	0.0446	0.267	down
Q61838	11287	ENSMUSG00C	Pzp			-4.196662	0.000421	0.00253	down
Q8BTM8	192176	ENSMUSG00C	Flna			-1.835946	0.0467	0.28	down
P28665	17836	ENSMUSG00C	Mug1			-1.894603	0.0434	0.26	down
Q61233	18826	ENSMUSG00C	Lcp1			-1.887831	0.0452	0.271	down
P10107	16952	ENSMUSG00C	Anxa1			-4.818541	0.041	0.246	down
P07759	20714	NA	Serpina3k			-2.687028	0.0451	0.27	down
Q61696	193740	1F	ENSMUSG00C	Hspala	Hs	-1.759362	0.00163	0.00977	down
Q8K183	216134	ENSMUSG00C	Pdxk			1.4106075	0.0213	0.128	up
Q9QYG0	29811	ENSMUSG00C	Ndr2			-1.002546	0.0439	0.263	down
Q61147	12870	ENSMUSG00C	Cp			-2.599425	0.048	0.288	down
Q00623	11806	ENSMUSG00C	Apoa1			-2.351599	0.046	0.276	down
P13020	227753	ENSMUSG00C	Gsn			-1.041349	0.00746	0.0448	down
Q8VCM7	99571	ENSMUSG00C	Fgg			-5.223086	0.0435	0.261	down
Q00612	14381	ENSMUSG00C	G6pdx			-1.449393	0.0211	0.126	down
070443	14687	ENSMUSG00C	Gnaz			2.0720626	0.00461	0.0277	up
P06909	12628	ENSMUSG00C	Cfh			-1.626662	0.0258	0.155	down
Q9CPW0	66797	NA	Cntnap2			-1.600495	0.00038	0.00228	down
P05555	16409	NA	Itgam			-3.477738	0.0222	0.133	down
Q9CZ30	67059	ENSMUSG00C	Ola1			-1.431831	0.0351	0.211	down
P11835	16414	NA	Itgb2			-2.956178	0.0284	0.17	down
Q62418	13169	ENSMUSG00C	Dbn1			-1.165289	0.0145	0.0869	down
P48318	14415	ENSMUSG00C	Gad1			1.1018826	0.00566	0.0339	up
Q9D7G0	19139	ENSMUSG00C	Prps1			-1.276001	0.00357	0.0214	down
Q99MN9	66904	ENSMUSG00C	Pccb			-3.187011	0.00271	0.0163	down
Q9JKF1	29875	ENSMUSG00C	Iqgap1			-4.293693	0.0299	0.18	down
Q8BIZ1	77531	NA	Anks1b			-1.587535	0.0096	0.0576	down
Q61176	11846	ENSMUSG00C	Arg1			-2.982718	0.0117	0.0704	down
Q9ET01	110095	ENSMUSG00C	Pyg1			-2.623126	0.0218	0.131	down
P27005	20201	ENSMUSG00C	S100a8			-3.516263	0.0485	0.291	down
Q8CGK7	14680	ENSMUSG00C	Gna1			-1.300264	0.00196	0.0118	down
P63158	15289	10C	ENSMUSG00C	Hmgbl1	Gm2	-5.986824	0.00109	0.00653	down
P54227	16765	ENSMUSG00C	Stmn1			-1.726061	0.000167	0.001	down
Q62059	13003	NA	Vcan			-1.234004	0.00407	0.0244	down
Q91VN4	66098	ENSMUSG00C	Chchd6			-2.775973	0.0104	0.0624	down
Q9CZT8	69908	ENSMUSG00C	Rab3b			-1.348222	0.0458	0.275	down
Q9WVA4	21346	ENSMUSG00C	Tagln2			-1.549734	0.0192	0.115	down
Q6URW6	71960	ENSMUSG00C	Myh14			1.4881134	0.0344	0.206	up
P21614	14473	ENSMUSG00C	Gc			-2.797736	0.033	0.198	down
Q61599	11857	ENSMUSG00C	Arhgdib			-3.737581	0.0307	0.184	down
P23953	13884	ENSMUSG00C	Ces1c			-3.597455	0.0383	0.23	down
Q99JI6	215449	ENSMUSG00C	Rap1b			1.4500241	0.0226	0.136	up
Q61702	16424	ENSMUSG00C	Itih1			-1.608903	0.0183	0.11	down
Q9CQX2	66427	ENSMUSG00C	Cyb5b			-1.220541	0.00943	0.0566	down
Q68FL6	216443	ENSMUSG00C	Mars			-1.199221	0.0124	0.0745	down
P42859	15194	NA	Htt			-1.133909	0.0339	0.203	down
P19221	14061	ENSMUSG00C	F2			-1.864458	0.0478	0.287	down
Q62393	21985	ENSMUSG00C	Tpd52			-1.230711	0.00146	0.00878	down
Q7TMY8	59026	ENSMUSG00C	Huwl			-2.664121	0.00643	0.0386	down
Q3U5Q7	22169	ENSMUSG00C	Cmpk2			-1.158989	0.0136	0.0817	down

Q9Z1Q5	114584	ENSMUSG00C	Clic1	-2.251477	0.0338	0.203 down
Q9CXS4	73139	ENSMUSG00C	Cenpv	-1.494529	0.0245	0.147 down
Q99LG2	212999	ENSMUSG00C	Tnp02	1.7233551	0.00365	0.0219 up
Q3TMH2	74616	ENSMUSG00C	Scrn3	1.9324724	0.000544	0.00326 up
P30681	97165	ENSMUSG00C	Hmgb2	-4.44639	0.0227	0.136 down
P01872	16019	NA	Ighm	-1.998248	0.014	0.0838 down
Q6P4T2	320632	ENSMUSG00C	Snrrp200	1.147363	0.0143	0.0861 up
Q9Z0H4	14007	ENSMUSG00C	Celf2	-1.253417	0.0197	0.118 down
P47791	14782	ENSMUSG00C	Gsr	-1.152682	0.0187	0.112 down
Q3UP87	50701	ENSMUSG00C	Elane	-3.93949	0.0416	0.25 down
Q80VP0	70381	ENSMUSG00C	Tecpr1	2.4089542	0.00121	0.00726 up
P49442	16329	ENSMUSG00C	Inpp1	1.0579182	0.00744	0.0446 up
Q8C166	266692	ENSMUSG00C	Cpne1	-1.171652	0.000619	0.00371 down
P07309	22139	ENSMUSG00C	Ttr	-4.353105	0.0238	0.143 down
Q6P5E4	320011	ENSMUSG00C	Uggt1	-1.119286	0.0107	0.064 down
Q64213	22668	NA	Sf1	1.2372371	0.0169	0.101 up
P51437	12796	ENSMUSG00C	Camp	-3.869739	0.0251	0.15 down
A2AQ25	208618	ENSMUSG00C	Et14	-1.007436	0.0321	0.193 down
Q61096	19152	NA	Prtn3	-2.763485	0.0303	0.182 down
P47962	100503670	ENSMUSG00C	Rp15	-1.591587	0.0267	0.16 down
Q6NS52	217480	NA	Dgkb	-1.323346	0.0237	0.142 down
Q3V132	73333	ENSMUSG00C	Slc25a31	1.5348712	0.00112	0.0067 up
Q9WV18	54393	ENSMUSG00C	Gabbr1	-2.894844	0.025	0.15 down
Q99K48	53610	ENSMUSG00C	Nono	-1.209455	0.0165	0.0992 down
Q8BR92	242481	ENSMUSG00C	Paln2	-1.039677	0.0123	0.074 down
Q9JKB1	50933	ENSMUSG00C	Uchl3	1.2996872	0.0111	0.0664 up
Q01405	20334	ENSMUSG00C	Sec23a	-1.663459	0.0334	0.2 down
P01864	380793	NA	Ighg2a	-4.00334	0.0185	0.111 down
Q05144	19354	ENSMUSG00C	Rac2	-4.8095	0.0315	0.189 down
Q9CZB0	66052	ENSMUSG00C	Sdhc	-1.762965	0.0207	0.124 down
Q3THW5	77605	ENSMUSG00C	H2afv	-1.558794	0.0105	0.0631 down
Q9JIF7	70349	ENSMUSG00C	Copb1	-1.753563	0.000876	0.00525 down
Q91V09	73447	ENSMUSG00C	Wdr13	-1.932981	0.00558	0.0335 down
P16045	16852	ENSMUSG00C	Lgals1	-2.0238	0.0104	0.0627 down
Q01339	11818	ENSMUSG00C	Apoh	-4.054454	0.0261	0.156 down
Q3U9G9	98386	ENSMUSG00C	Lbr	-2.311841	0.0363	0.218 down
Q9DC16	67458	ENSMUSG00C	Ergic1	-1.834019	0.0214	0.128 down
P06800	NA	NA	NA	-3.21514	0.0391	0.235 down
P39447	21872	ENSMUSG00C	Tjp1	-1.242128	0.00648	0.0389 down
P58404	97387	ENSMUSG00C	Strn4	-2.013346	0.0102	0.0609 down
P59325	217869; 1C	ENSMUSG00C	Eif5; LOC1	-1.041222	0.00903	0.0542 down
Q8COL0	52837	ENSMUSG00C	Tmx4	-1.283934	0.00671	0.0403 down
Q3B7Z2	76303	ENSMUSG00C	Osbp	-1.382279	0.0242	0.145 down
P61222	24015	ENSMUSG00C	Abce1	-1.627304	0.0122	0.0731 down
Q8BJ42	244310	ENSMUSG00C	D1gap2	1.4546025	0.00058	0.00348 up
Q8VDP4	219158	ENSMUSG00C	2610301G19	-1.057374	0.0138	0.0826 down
Q6NVF9	432508	ENSMUSG00C	Cpsf6	-2.77742	0.0123	0.0737 down
Q80TM9	64652	ENSMUSG00C	Nisch	-1.579249	0.00971	0.0583 down
Q9QXT0	56530	ENSMUSG00C	Cnpy2	-2.673597	0.000529	0.00317 down
Q4VAE3	74868	ENSMUSG00C	Tmem65	-1.45075	0.00453	0.0272 down
Q61205	18476	ENSMUSG00C	Pafah1b3	1.1617359	0.0141	0.0844 up

035350	12333	ENSMUSG00(Capn1	-2.409046	0.012	0.0722 down
Q91YI0	109900	ENSMUSG00(Asl	-1.115503	0.0145	0.0867 down
P63082	11984;	10CENSMUSG00(Atp6v0c; f	1.3810479	0.00598	0.0359 up
Q9Z1J3	18041	ENSMUSG00(Nfs1	-1.798314	0.000451	0.00271 down
Q9ERI6	105014	ENSMUSG00(Rdh14	-1.460606	0.0456	0.273 down
Q7TQ95	69605	ENSMUSG00(Lnp; Lnpk	-2.551429	0.014	0.0841 down
035857	21856	ENSMUSG00(Timm44	1.7054544	0.0136	0.0818 up
Q9DBG5	66905	ENSMUSG00(Plin3	-2.569172	0.0231	0.138 down
Q8BSS9	327814	NA Ppfia2	1.0921188	0.0144	0.0863 up
Q9EQZ6	56508	ENSMUSG00(Rapgef4	-1.558502	0.00186	0.0112 down
Q8OX50	74383	ENSMUSG00(Ubap21	-1.336082	0.0361	0.216 down
P60229	16341	ENSMUSG00(Eif3e	-1.310566	0.000378	0.00227 down
088587	12846	ENSMUSG00(Comt	1.8072493	0.0137	0.0821 up
Q8VBW6	234664	ENSMUSG00(Nae1	-1.150327	0.0106	0.0637 down
Q9D1Q6	76299	ENSMUSG00(Erp44	-1.484043	0.0129	0.0772 down
Q9Z0U1	21873	ENSMUSG00(Tjp2	-1.189715	0.0123	0.074 down
Q9DAK9	75454	ENSMUSG00(Phpt1	-1.311356	0.005	0.03 down
P07310	12715	ENSMUSG00(Ckm	1.1545705	0.0266	0.16 up
Q8VDL4	72141	NA Adpgk	-2.707279	0.0372	0.223 down
Q9DBZ5	73830	ENSMUSG00(Eif3k	-1.297094	0.0336	0.201 down
Q9DB60	66469	ENSMUSG00(2810405K02	-1.026145	0.0114	0.0682 down
Q91VT4	234309	ENSMUSG00(Cbr4	-1.569321	0.0473	0.284 down
Q9Z0E6	14469	ENSMUSG00(Gbp2	-1.92553	0.0294	0.176 down
Q62523	22793	ENSMUSG00(Zyx	-1.666114	0.029	0.174 down
Q99KB8	14651	NA Hagh	-1.206572	0.0201	0.12 down
Q69ZS6	75209	ENSMUSG00(Sv2c	-2.101287	0.0385	0.231 down
Q62426	13014	ENSMUSG00(Cstb	-1.616725	0.0171	0.103 down
Q99MR6	83701	ENSMUSG00(Srrt	1.4008814	0.0248	0.149 up
Q61730	16180	ENSMUSG00(Illrap	-1.385644	0.0249	0.15 down
Q6KAR6	211446	ENSMUSG00(Exoc3	-1.23821	0.0485	0.291 down
Q9QXB9	13495	ENSMUSG00(Drg2	-4.272071	0.002	0.012 down
Q9QYI3	56354	ENSMUSG00(Dnajc7	-1.095199	0.0245	0.147 down
Q80UP3	104418	ENSMUSG00(Dgkz	-2.742226	0.000556	0.00333 down
Q9ERT9	58200	ENSMUSG00(Ppp1rla	1.3946803	0.00806	0.0483 up
Q8K010	75475	ENSMUSG00(Oplah	-1.485715	0.0315	0.189 down
P32261	11905	ENSMUSG00(Serpinc1	-3.244801	0.0412	0.247 down
Q99NB1	68738	ENSMUSG00(Acss1	-1.2823	0.0209	0.126 down
P09813	11807	ENSMUSG00(Apoa2	-3.230534	0.0433	0.26 down
Q80VC9	69697	ENSMUSG00(Camsap3	-1.557448	0.021	0.126 down
Q99JG2	171469	ENSMUSG00(Gpr3711	-1.847964	0.0102	0.061 down
P18894	13142	NA Dao	1.5763776	0.00339	0.0203 up
Q9CQE1	66536	ENSMUSG00(Nipsnap3b	-1.715242	0.0128	0.0769 down
Q9D6Y7	110265	ENSMUSG00(Msra	-1.254891	0.049	0.294 down
P15327	12183	ENSMUSG00(Bpgm	-1.595146	0.00259	0.0155 down
Q9WUD1	56424	ENSMUSG00(Stub1	1.0412252	0.0208	0.125 up
Q9CY50	107513	ENSMUSG00(Ssr1	-1.21073	0.000843	0.00506 down
Q9JJY3	58994	ENSMUSG00(Smpd3	1.3876069	0.000636	0.00382 up
Q8BNU0	76813	ENSMUSG00(Armc6	2.4256749	0.00178	0.0107 up
P70460	22323	ENSMUSG00(Vasp	-3.61219	0.0168	0.101 down
008992	53378	ENSMUSG00(Sdcbp	2.2582553	0.0338	0.203 up
Q921W4	66609	ENSMUSG00(Cryz11	-1.407587	0.0434	0.26 down

Q9WTX2	23992	ENSMUSG00CPrkra	2.738459	0.00755	0.0453 up
Q8C8T8	69499	NA Tsr2	2.3786824	0.00536	0.0322 up
Q99J36	233802	ENSMUSG00CThumpd1	-1.366075	0.0498	0.299 down
Q8K1L5	76497	NA Ppplr11	-1.507122	0.00608	0.0365 down
Q01730	20163	NA Rsul	1.7046185	0.00239	0.0143 up
Q5M8N4	NA	NA NA	1.9123408	0.00809	0.0485 up
Q9EPR5	81840	ENSMUSG00CSorcs2	-2.44633	0.00515	0.0309 down
Q8VE62	218693	ENSMUSG00CPaip1	-1.038089	0.0182	0.109 down
Q61239	14272	ENSMUSG00CFnta	-2.246488	0.00721	0.0432 down
O55135	16418	ENSMUSG00CEif6	-3.224043	0.0144	0.0862 down
Q9CQ10	66700	ENSMUSG00CChmp3	-2.025184	0.0409	0.245 down
Q9DCT1	56043	ENSMUSG00CAkr1e1	-1.513334	0.0203	0.122 down
P17665	12867; 654	ENSMUSG00CCox7c; Gm1	-1.027919	0.0429	0.257 down
P50136	12039	NA Bckdha	1.9517135	0.0443	0.266 up
Q99NF2	56876	ENSMUSG00CNelf; Nsmf	-3.210885	0.000547	0.00328 down
Q8BHK1	233280	ENSMUSG00CNipa1	-1.976342	0.00446	0.0267 down
Q8VE22	64656	ENSMUSG00CMrps23	1.6358579	0.0222	0.133 up
P63089	19242	ENSMUSG00CPtn	-1.065406	0.0254	0.152 down
P06880	14599	ENSMUSG00CGh	-3.142823	0.0378	0.227 down
P62305	20643	ENSMUSG00CSnrpe	1.1291273	0.025	0.15 up
P56565	20193	NA S100a1	2.1412334	0.000683	0.0041 up
Q9D2N9	77573	ENSMUSG00CVps33a	-1.389529	0.00291	0.0175 down
Q3TCN2	71772	ENSMUSG00CP1bd2	-1.856771	0.00198	0.0119 down
B1AR13	217149	ENSMUSG00CCisd3	1.5963994	0.00011	0.000662 up
Q9D967	67881	ENSMUSG00CMdp1	1.189296	0.00777	0.0466 up
O35459	51798	ENSMUSG00CEch1	-1.423175	0.0185	0.111 down
Q64511	21974	ENSMUSG00CTop2b	2.1186399	0.0231	0.139 up
O54781	20817	NA SrpK2	1.5890648	0.0104	0.0625 up
Q9D0A3	70420	ENSMUSG00C2610034B18	-1.16392	0.000481	0.00288 down
Q8BWS5	243385	ENSMUSG00CGprin3	-2.793058	0.00717	0.043 down
P62309	68011	ENSMUSG00CSnrpg	-2.001518	0.0015	0.00899 down
Q80WQ2	234729	ENSMUSG00CVac14	1.2604916	0.000197	0.00118 up
Q8K426	245195	ENSMUSG00CRetnlg	-1.676062	0.0249	0.149 down
P97952	20266	ENSMUSG00CScn1b	-3.461152	0.00612	0.0367 down
Q9WUB4	22428	ENSMUSG00CDctn6	1.0299834	0.0147	0.0882 up
Q9JHL1	65962	NA Slc9a3r2	-1.802869	0.00238	0.0143 down
P59708	66055	ENSMUSG00C0610009D07	2.326145	0.00307	0.0184 up
Q9D4H1	66482	ENSMUSG00CExoc2	-2.159314	0.000606	0.00363 down
O88735	17761	NA Map7; Mtaf	-1.897358	0.031	0.186 down
Q9D6S7	67871	ENSMUSG00CMrrf	2.2308582	0.0279	0.168 up
Q06335	11804	ENSMUSG00CAplp2	-3.806971	0.000967	0.0058 down
P47743	14823	ENSMUSG00CGrm8	1.0481418	0.00443	0.0266 up
Q3TC33	67433	ENSMUSG00CCcdc127	1.4717923	0.0215	0.129 up
Q9ROM6	56382	ENSMUSG00CRab9	-1.547322	0.00343	0.0206 down
P53702	15159	ENSMUSG00CHccs	-1.265621	0.0142	0.0855 down
Q9Z1K5	23806	ENSMUSG00CArih1	-1.795791	0.0157	0.0939 down
Q9Z2D1	77116	ENSMUSG00CMtmr2	1.4537486	0.00312	0.0187 up
Q99LB7	192166	ENSMUSG00CSardh	1.5715842	0.000348	0.00209 up
Q9ER35	63828	ENSMUSG00CFn3k	1.3219223	0.00217	0.013 up
Q00519	22436	ENSMUSG00CXdh	1.2348119	0.0317	0.19 up
Q9Z2V5	15185	ENSMUSG00CHdac6	1.3695523	0.00137	0.00821 up

P21300	11997	ENSMUSG00C	Akr1b7	-1.031232	0.0296	0.177 down
Q9QYF1	17252	ENSMUSG00C	Rdh11	-1.027108	0.00529	0.0317 down
Q9DC63	57443	ENSMUSG00C	Fbxo3	-1.92199	0.0211	0.127 down
Q7TNC4	192196	ENSMUSG00C	Luc712	-1.446461	0.0158	0.0951 down
Q3UYG8	72899	ENSMUSG00C	MacroD2	-2.142741	0.0138	0.083 down
Q61462	13057	ENSMUSG00C	Cyba	-1.488409	0.0227	0.136 down
P59759	239719	NA	Mk12	-5.776771	0.0123	0.074 down
P56212	59046	ENSMUSG00C	Arpp19	-1.965753	0.000872	0.00523 down
Q91YQ3	105859	ENSMUSG00C	Csdc2	1.4487528	0.00255	0.0153 up
Q8BYI8	74525	ENSMUSG00C	8430419L09	1.1023969	0.00049	0.00294 up
Q8VC42	76482	ENSMUSG00C	3110002H16	1.4285492	0.0297	0.178 up
O88845	56697	ENSMUSG00C	Akap10	1.6506329	0.000212	0.00127 up
Q3UHH2	73102	ENSMUSG00C	Slc22a23	-1.163342	0.00755	0.0453 down
Q60780	14457	NA	Gas7	-1.638606	0.0484	0.29 down
Q8C7D2	58799	ENSMUSG00C	Crbn	1.2299186	0.00347	0.0208 up
O55057	18582	ENSMUSG00C	Pde6d	1.3869579	0.000117	0.000704 up
Q9CXV1	66925	ENSMUSG00C	Sdhd	-2.087069	0.0393	0.236 down
Q8R395	66398	NA	CommD5	1.0355458	0.00188	0.0113 up
Q9D289	78232	ENSMUSG00C	Trappc6b	1.9819799	0.00645	0.0387 up
P00158	17711; 333	ENSMUSG00C	CYTb	1.2073603	0.00074	0.00444 up
Q8VCM8	103425	ENSMUSG00C	Ncln	1.4502889	0.0139	0.0832 up
P61458	13180	ENSMUSG00C	Pcbd1	-1.455454	0.00556	0.0334 down
Q3V038	69480	ENSMUSG00C	Ttc9	-1.444967	0.0253	0.152 down
Q8C2E7	223593	ENSMUSG00C	E430025E21	1.2383117	0.0292	0.175 up
P69566	56705	NA	Ranbp9	2.2355521	0.0349	0.209 up
P70403	13047	NA	Cux1	1.444921	0.0319	0.191 up
Q8CDU6	226098	ENSMUSG00C	Hectd2	1.00429	0.00322	0.0193 up
Q8VHK9	72162	ENSMUSG00C	Dhx36	1.3552357	0.00294	0.0176 up
Q99N94	78523	ENSMUSG00C	Mrpl9	1.3636266	0.0115	0.0692 up
Q9CQS8	66212	ENSMUSG00C	Sec61b	-1.307809	0.0235	0.141 down
Q9D387	76161	ENSMUSG00C	Lamp5	1.6355638	0.0457	0.274 up
Q9ET22	83768	ENSMUSG00C	Dpp7	1.4270379	0.00074	0.00444 up
Q9ESZ8	14886	ENSMUSG00C	Gtf2i	1.8194526	0.011	0.0659 up
Q9ERR7	93684	NA	Sep15; Sel1	1.5160585	0.0472	0.283 up
Q6GYP7	56784	ENSMUSG00C	Ralgap1	1.7952365	0.0274	0.165 up
Q91X56	94226	ENSMUSG00C	Slpr5	1.6642691	0.000103	0.000619 up
Q9R112	59010	ENSMUSG00C	Sqrd1; Sqc	-1.691798	0.0133	0.0801 down
Q8CIV8	70430	ENSMUSG00C	Tbce	1.0351649	0.00448	0.0269 up
P23090	NA	NA	NA	1.1025474	0.00053	0.00318 up
Q9D826	19193	ENSMUSG00C	Pipox	1.5929748	0.0164	0.0984 up
B2RUJ5	319924	ENSMUSG00C	Apb1	3.4976881	0.00838	0.0503 up
Q80XG9	243499	ENSMUSG00C	Lrrtm4	1.8754396	0.00152	0.00913 up
Q69ZX8	319713	ENSMUSG00C	Ablim3	1.0808532	0.0218	0.131 up
Q8VEA4	72170	ENSMUSG00C	Chchd4	1.1200809	0.0104	0.0626 up
Q9CR76	66690	ENSMUSG00C	Tmem186	1.9404184	0.00267	0.016 up
P56213	11692	ENSMUSG00C	Gfer	-1.518523	0.0169	0.101 down
P03903	17720; 333	ENSMUSG00C	ND4L	1.0602195	0.0267	0.16 up
Q9DB50	108012	ENSMUSG00C	Ap1s2	3.6972469	0.0212	0.127 up
Q91VU0	27999	ENSMUSG00C	Fam3c	2.7144359	0.000287	0.00172 up
Q8VEB4	192654	ENSMUSG00C	Pla2g15	1.2856069	0.0279	0.168 up
Q9D6F4	14397	ENSMUSG00C	Gabra4	1.0275244	0.0317	0.19 up

Q8CE90	26400 ENSMUSG00CMap2k7	1.1060732	0.01	0.0601 up
Q9CZX7	72519 ENSMUSG00C Tmem55a	-1.065626	0.0313	0.188 down

Accession	Entrez	Gene	Ensembl	Gene	Sym	log2FC	p. value	p. adjust.	direction
O08599	20910	ENSMUSG00C	Stxbp1			-1.089388	0.0135532	0.5605597	down
Q9ERD7	22152	ENSMUSG00C	Tubb3			-1.698064	0.0029378	0.5605597	down
P61982	22628	ENSMUSG00C	Ywhag			-1.298326	0.023082	0.5605597	down
P08249	17448	ENSMUSG00C	Mdh2			-1.925963	0.0220373	0.5605597	down
P68510	22629	ENSMUSG00C	Ywhah			-1.124814	0.0355255	0.5605597	down
P14152	17449	ENSMUSG00C	Mdh1			-1.406065	0.0124585	0.5605597	down
P18760	12631	ENSMUSG00C	Cf11			-1.360619	0.0249473	0.5605597	down
Q920I9	104082	ENSMUSG00C	Wdr7			1.7124286	0.0346641	0.5605597	up
P09528	14319	ENSMUSG00C	Fth1			-1.108161	0.015425	0.5605597	down
P28663	17957	ENSMUSG00C	Napb			-1.632112	0.0082812	0.5605597	down
P63024	22319	ENSMUSG00C	Vamp3			2.2393148	0.0245863	0.5605597	up
O35098	26757		Dpysl4			-1.711211	0.0482246	0.5605597	down
Q01853	269523	ENSMUSG00C	Vcp			1.0941875	0.0454886	0.5605597	up
P14231	11932	ENSMUSG00C	Atplb2			-1.901788	0.0391097	0.5605597	down
P05132	18747	ENSMUSG00C	Prkaca			1.4307088	0.043968	0.5605597	up
Q9R111	14544	ENSMUSG00C	Gda			-1.303626	0.0362251	0.5605597	down
Q80UG5	53860	ENSMUSG00C		9-Sep		-1.739066	0.0161629	0.5605597	down
P45591	12632	ENSMUSG00C	Cf12			-2.016516	0.0149744	0.5605597	down
Q8CBH5	98682	ENSMUSG00C	Mfsd6			1.50466	0.036483	0.5605597	up
Q8BU14	69276	ENSMUSG00C	Sec62			1.7206499	0.0398114	0.5605597	up
Q80YA3	114874		Ddhd1			1.893265	0.0046446	0.5605597	up
P47754	12343	ENSMUSG00C	Capza2			-1.860788	0.0354138	0.5605597	down
O70145	17970	ENSMUSG00C	Ncf2			-1.684982	0.0042812	0.5605597	down
O88685	19182	ENSMUSG00C	Psmc3			1.0895305	0.0039137	0.5605597	up
Q9QYE3	14025	ENSMUSG00C	Bcl11a			1.0402102	0.0230681	0.5605597	up
Q8C5H8	68646	ENSMUSG00C	Nadk2; Nac			-1.116742	0.0137187	0.5605597	down
Q5XJE5	235497	ENSMUSG00C	Leo1			1.6268479	0.0111222	0.5605597	up
O55029	50797	ENSMUSG00C	Copb2			1.4411263	0.0095804	0.5605597	up
Q80TL7	67074	ENSMUSG00C	Mon2			1.820425	0.0307518	0.5605597	up
Q6P4T2	320632	ENSMUSG00C	Snrnp200			2.0970093	0.0336813	0.5605597	up
Q811D0	13383	ENSMUSG00C	Dlg1			1.0893764	0.0006464	0.3937941	up
Q8JZQ2	69597	ENSMUSG00C	Afg3l2			-2.040302	0.0199168	0.5605597	down
Q80YV2	232679	ENSMUSG00C	Zc3hc1			4.0708234	0.0286952	0.5605597	up
Q91VN4	66098	ENSMUSG00C	Chchd6			-2.162281	0.0170803	0.5605597	down
B9EJ80	107368	ENSMUSG00C	Pdzd8			1.6700126	0.0288419	0.5605597	up
Q3TWL2	219024	ENSMUSG00C	Tmem55b			1.5635014	0.0202896	0.5605597	up
Q9D2V7	78885	ENSMUSG00C	Coro7			-2.057354	0.0102673	0.5605597	down
BOV2N1	19280	ENSMUSG00C	Ptprs			-1.276306	0.0469507	0.5605597	down
Q61410	19092		Prkg2			1.2201406	0.0004423	0.3937941	up
Q64105	20751		Spr			-2.012834	0.0219064	0.5605597	down
Q64674	20810	ENSMUSG00C	Srm			-1.112233	0.0087262	0.5605597	down
Q6ZWU9	57294; 10C	ENSMUSG00C	Rps27; Gm			-1.044048	0.0207484	0.5605597	down
Q6PNC0	240283	ENSMUSG00C	Dmxl1			1.0973368	0.0430666	0.5605597	up
Q8CHP8	67078	ENSMUSG00C	Pgp			-1.863814	0.0279975	0.5605597	down
Q921J2	19744	ENSMUSG00C	Rheb			-4.848102	0.015086	0.5605597	down
Q62393	21985	ENSMUSG00C	Tpd52			-1.01293	0.0128543	0.5605597	down
Q69ZR9	218850		D14Abbl1e;			-1.90138	0.0056368	0.5605597	down
Q9WV54	11886	ENSMUSG00C	Asah1			-3.010298	0.034621	0.5605597	down
Q8VE88	67726	ENSMUSG00C	Fam114a2			1.6252407	0.0110408	0.5605597	up
P27659	27367	ENSMUSG00C	Rp13			3.5291038	0.0399089	0.5605597	up

Q80U63	170731	ENSMUSG00C	Mfn2	1.9016177	0.0383257	0.5605597	up
POC913	69784	ENSMUSG00C	1500009L16	1.7665998	0.0354231	0.5605597	up
Q3U0S6	69903	ENSMUSG00C	Rasip1	1.0201743	0.009086	0.5605597	up
B2RQC6	69719	ENSMUSG00C	Cad	1.3168462	0.0021705	0.5605597	up
O35683	54405	ENSMUSG00C	Ndufa1	-1.952188	0.0150861	0.5605597	down
P97384	11744	ENSMUSG00C	Anxa11	-1.898146	0.0072172	0.5605597	down
Q9WUH1	56395	ENSMUSG00C	Tmem115	-1.640199	0.0066977	0.5605597	down
Q9ESJ1	63955	ENSMUSG00C	Cables1	1.8578184	0.0206352	0.5605597	up
P61514	19981	ENSMUSG00C	Rpl37a	3.4384779	0.0470074	0.5605597	up
Q80XP8	72826	ENSMUSG00C	Fam76b	1.2696532	0.0314663	0.5605597	up
P38060	15356	ENSMUSG00C	Hmgcl	-1.133734	0.0335542	0.5605597	down
Q9D1M0	110379	ENSMUSG00C	Sec13	-1.028019	0.0236634	0.5605597	down
Q60592	17776		Mast2	1.1399822	0.0087666	0.5605597	up
Q8BWY3	225363	ENSMUSG00C	Etf1	-1.626116	0.0425579	0.5605597	down
P47867	20255	ENSMUSG00C	Scg3	1.4082927	0.0203223	0.5605597	up
Q9QY76	56491		Vapb	1.294663	0.0017874	0.5605597	up
Q9EPK7	65246	ENSMUSG00C	Xpo7	-1.913628	0.0261717	0.5605597	down
Q6NTA4	245670	ENSMUSG00C	Rragb	1.3051323	0.0128131	0.5605597	up
Q6PEB6	19070	ENSMUSG00C	Mob4	-1.681915	0.0048933	0.5605597	down